Neuropilin-1 directs PDGFRα-entry into lung fibroblasts and signaling from very early endosomes

Stephen E. McGowan and Diann M. McCoy

Department of Veterans Affairs Research Service and Department of Internal Medicine, University of Iowa Carver College of Medicine, Iowa City, Iowa USA

Running title: Neuropilin-1 regulates PDGFRα endosomal signaling

Key words: alveolar development, emphysema, signaling endosome, myofibroblast

SEM conceived, designed and performed experiments, analyzed data, and wrote the manuscript. DMM performed experiments, analyzed data, and edited the manuscript.

Address correspondence to

Stephen McGowan M.D.
Division of Pulmonary, Critical Care, and Occupational Medicine
C33B GH
Department of Internal Medicine
University of Iowa Hospitals and Clinics
200 Hawkins Dr.
Iowa City, Iowa 52242
stephen-mcgowan@uiowa.edu
Phone 319-356-1013

Abstract

Platelet-derived growth factor receptor alpha (PDGFRα) is absolutely required for the development of secondary pulmonary alveolar septa. Our earlier observations indicated that PDGFRα resides intracellularly as well as on the plasma membrane of murine lung fibroblasts (LF). We have examined how neuropilin-1 (Nrp1), a surface receptor without kinase activity, regulates the intracellular trafficking of PDGFRα in LF obtained from mice, some bearing a targeted deletion of Nrp1 in myofibroblasts. Using the proximity ligation assay we observed that PDGFRα and Nrp1 co-localized in both early antigen-1 (EEA1) containing sorting endosomes and with adaptor protein containing a pleckstrin homology domain and a phosphotyrosine-binding domain-1 (APPL1) in very early endosomes (VEE). These findings were confirmed using live cell imaging, which demonstrated that recently internalized PDGFRα was observed in Rab5-containing vesicles residing within 100 nm of the plasma membrane. Nrp1-deletion reduced the phosphorylation of Akt, (protein kinase B) the major downstream target of PDGFRα, and limited accumulation of inositol-3phosphates in APPL1-containing endosomes after exposure to PDGFA. PDGFRα co-immunoprecipitated with APPL1, indicating that PDGFRα enters VEE. Targeted deletion of Nrp1 or APPL1-depletion in control LF reduced the activity of an Akt1 biosensor following stimulation with PDGFA. Our findings demonstrate that Nrp1 enhances the entry of PDGFRα into APPL1 containing VEE and that APPL1 enhances PDGFRα-signaling. Therefore, Nrp1 promotes endosomal signaling by PDGFRα offering a potential mechanism to explain our prior observation that Nrp1 supports the formation of alveolar ducts and alveoli during secondary septation in mice.

Introduction

In mammals birth heralds the rapid expansion of the pulmonary gas-exchange surface through secondary septation, when sheets of tissue subdivide rudimentary air sacs demarcated by the primary septa. In mice, on postnatal day 4 (P4) mesenchymal cells occupying septal crests begin to extend from the primary septa into the distal air sacs (1). There is limited understanding of the cellular mechanisms which regulate the coordinated extension of these thin sheets of tissue containing epithelial, endothelial and mesenchymal cells. However, it is known that the mesenchymal cells, which initially occupied the septal crests, are very similar to those which later occupy the distal septal tips. These cells reside near a capillary loop, adjacent to dense deposits of elastin and collagen, contain α-smooth muscle actin (αSMA, ACTA2), and express platelet-derived growth factor-α (PDGFRα) (21) (29). By inference, relocation of this population of mesenchymal cells bearing characteristics of myofibroblasts (MF) suggests that they migrate during secondary septation. However, because cellular movement cannot be directly observed in the lung in real time, our current understanding comes from characterization of specific-gene deletions which disrupt secondary septation, and from studying cultured lung fibroblasts (LF).

Mesenchymal cells bearing platelet-derived growth factor-α (PDGFRα), the sole receptor for PDGFA, are absolutely required, because deletion of either PDGFRα or PDGFA results in failure of secondary septation, marked by an absence of αSMA expressing cells and elastic fibers at septal tips (5). Although it was initially proposed that PDGFRα-signaling mainly regulated the expansion and differentiation of a MF-lineage, it is now clear that PDGFRα is a marker rather than a distinct determinant of this lineage (24) (23). Ongoing PDGFRα-signaling is required to sustain proliferation of MF and temper septal thinning, which accompanies maturation of the alveolar capillary network (30) (1). Studies in primary cultures of neonatal mouse lung fibroblasts (LF) indicate that PDGFA and PDGFRα stimulate migration and mediate mechano-responsiveness to substrate rigidity (33). The size of the intracellular pool of PDGFRα exceeds that displayed on the cell-surface prompting us to examine whether intracellular receptors are important for signaling (31).

Other receptor tyrosine kinases (RTK) signal from endosomes, thereby regulating cell-polarity and migration (3). The most extensively studied entry portal from the plasma membrane involves sequestration in clathrin-coated pits and internalization through dynamin-mediated excision. The RTK ligand-binding domain is usually contained within the vesicle whereas the kinase-domain is oriented outward into the cytoplasm. Initial sorting reflects modulatory interactions between inositol phosphates, small GTPases including Ras-analog in brain (Rab)35 and Arf6, which direct cargo to Rab5 positive endosomes, from whence the cargo may enter early antigen-1 (EEA1, a Rab effector)-containing sorting endosomes (early endosomes) (44) (14). Alternatively, the cargo may segregate to adaptor protein containing a pleckstrin homology domain and a phosphotyrosine-binding domain-1 (APPL1)-containing very early (signaling) endosomes (VEE) (9). Once in the sorting endosome, cargo can be recycled back to the plasma membrane via Rab4 (short route) or Rab11 (long route) containing endosomes or alternatively ubiquitinated, dephosphorylated and transferred to Rab7-containing multi-vesicular bodies (then ultimately to lysosomes) (10).

Endosomal recycling of PDGFRs (more extensively for PDGFRβ) was studied in non-transformed fibroblasts, in which phosphorylated PDGFRβ was internalized via clathrin-dependent and independent mechanisms, entered sorting endosomes, moved to Rab4-containing vesicles, and returned to the plasma membrane (17). In contrast to PDGFRβ, PDGFRα was internalized but did not recycle unless it had heterodimerized with PDGFRβ.

Because the intracellular trafficking of PDGFRα remains largely undefined, we studied the endosomal distribution of PDGFRα within neonatal pulmonary LF, where it is a critical regulator of cell proliferation and migration. We sought to determine whether PDGFRα actively signals from endosomes following internalization. Very early endosomes, which contain APPL1 and/or APPL2, are located immediately beneath the plasma membrane and preserve active RTK-signaling intracellularly (9). We and others have shown that deletion of neuropilin-1 (Nrp1) in alveolar mesenchymal cells disrupts alveolar septation, reduces LF-migration and blunts mechano-sensitivity to rigid substrates (34) (26). Neuropilin-1 is a

transmembrane receptor without kinase activity which promotes signaling by class 3 semaphorins and vascular endothelial growth factor-A (VEGF-A)-165, and PDGFRα (53) (36) (2). The carboxyl terminus of Nrp1 includes a SEA-domain which binds the pleckstrin-homology (PH) domain of GIPC1 (G protein-α interacting protein-1, synectin). GIPC1 associates with APPL1 and myosin-6 (Myo6), a non-canonical myosin motor which moves towards the actin plus-end, thereby carrying endosomal cargo towards the interior of the cell (50) (28). Myosin-6 supports the function of signaling endosomes during formation of filopodia, podosomes, and lamellipodia, which each enable the cell to probe its extracellular contacts during migration (27).

We hypothesized that Nrp1 promotes PDGFRα-signaling from APPL1-containing VEE. To address this hypothesis using LF isolated from mice bearing specific MF-targeted gene-deletions, we have examined how PDGFA, and targeted deletions of PDGFRα or Nrp1 modify the colocalization of PDGFRα or Nrp1 with APPL1 and influence PDGFRα-signaling.

Materials and Methods

Isolation of lung fibroblasts. Lung fibroblasts (LF) were isolated for culture at postnatal day (P)10 or P12 from mice of either gender with the following genotypes: TGCre+/-;PDGFRαF/F, TGCre+/-;Nrp1F/F (the heterozygous *tagln*-Cre allele excises LoxP-flanked segment of *pdgfrα* or *nrp1* DNA; and from littermate TGCre+/-;PDGFRαF/- or TGCre+/-;Nrp1F/- (only one *nrp1* LoxP flanked allele) (34). Protocols for animal use were approved by the Iowa City Veterans Affairs Medical Center animal use committee (32). The pulmonary parenchymal mesenchymal cells (which will be referred to as LF although they may be partially comprised of pericytes) were isolated using a previously reported method involving digestion with collagenase (30). The LF were selected from the dispersed cells by their adherence to tissue culture dishes for 1h at 37^{o}C. Nearly all endothelial and epithelial cells fail to adhere during this short period. Non-adherent cells were removed by serial washes with PBS, prior to releasing the adherent cells with TrypLE Express®. The purity of the released LF population has previously been assessed by immunostaining for cellular markers specific for epithelial (anti-pan cytokeratin antibody),

128 macrophage (CD 206) and endothelial (CD31) cells (30). Epithelial and endothelial cells comprised
129 approximately 2.5 and 1.6 % respectively (30).

130 *Plasmids, transfection and baculovirus transduction*. Plasmids were obtained from Addgene
131 (Watertown, MA) and are listed in Supplementary Table 1, with acknowledgement of the donating
132 investigators. Traditional cloning methods were used to replace portions within some of the plasmids to
133 insert the desired fluorescent reporter. mRuby3 within Addgene 105780 was amplified by PCR to
134 introduce a 5' NheI and 3' XhoI sites for cloning into the vector containing APPL1 (27683) from which
135 mCherry had been excised using NheI and XhoI. The Nrp1 coding region of 21934 was excised with
136 AgeI and inserted into the AgeI site of 105795 5' to mClover3. The PDGFRα coding region was excised
137 from 66787 using HindIII and KpnI and inserted into the multiple cloning site pCMV-(DYKDDDDK)-N
138 (Takara Bio. Mountain View, CA) after digestion with HindIII and KpnI. The various vectors were
139 dephosphorylated with Antarctic phosphatase New England Biolabs (NEB, Ipswich, MA) prior to
140 ligation. The AktAR2 and AktPH-GFP biosensors were used as supplied by Addgene, without
141 modification. Plasmid DNA was purified using EndoFree Plasmid Maxi-Prep (Qiagen Germantown,
142 MD) purification system and introduced into cultures of primary LF isolated from mice with the genotype
143 of interest using Lipofectamine 3000 (ThermoFisher, Waltham MA) or Transit IT 2020 (Mirus Bio
144 Madison, WI) following the manufacturers' instructions. Early endosomes were labeled with CellLight®
145 (ThermoFisher C10586, Rab5-GFP) and late endosomes were labeled with CellLight® (ThermoFisher
146 C10589, Rab7-RFP). Sub-confluent monolayers were transduced with Baculovirus for 3 h at 25^{o} in
147 Leibovitz's L15 medium containing 1% FBS, 2 mM sodium butyrate, 2 mg/ml glucose, 100 U/ml
148 penicillin and 100 μg/ml streptomycin) 24 h prior to imaging.

149 *Confocal microscopy*. PDGFRα was co-localized with Rab5 or Rab7 (introduced through Baculovirus
150 transduction)-containing vesicles or with APPL1, which was introduced by plasmid-transfection. To
151 achieve sufficient resolution, endosomal vesicles were imaged using spinning-disk confocal microscopy.
152 The "antibody feeding assay" was used to attach a fluorescence-conjugated anti-DYKDDDDK antibody

to the exposed PDGFRα-N-terminal DYKDDDDK on LF, which had been transfected with pCMV-PDGFRα –DYKDDDDK (37). After allowing the antibody to attach and washing at 4^{o}, PDGFA was added and the cells were warmed to 37^{o} immediately prior to imaging. Live-imaging was performed using an Olympus IX81 inverted microscope equipped with a DSU disk scanning unit, and an Excelitas X-Cite 120 LED light source. The LF were maintained at 37^{o} in medium comprised of a 1:1 mix Leibovitz L15:FluroBrite™ medium containing 1% FBS, 30 mM HEPES 1 mM $CaCl_2$, and 100 U/ml penicillin and 100 μg/ml streptomycin, in a humidified atmosphere of 10% CO2, 21% oxygen and 69% nitrogen. Cells were visualized using DIC (Olympus UPLSAPO60XS2 silicone oil objective) to exclude any with large vacuoles or lacking a smooth cellular boundary (to exclude less viable cells), and an image was captured. The z-plane for this image was set as a middle of a 0.5 μm interval z-stack extending 1 μm above and below this level. Images were captured using a Hamamatsu OrcaR2 CCD camera, the z-stacks were converted to Tif-format and the image that was optimally focused was selected for analysis. Optimized images of 10 to 12 different LF were analyzed for each condition after acquisition over a period of 30 minutes following the addition of 25 ng/ml PDGFA or its diluent.

To assess the accumulation of PDGFRα in lysosomes, leupeptin was added to the cultures 3h prior to exposure to 25 ng/ml PDGFA to enable accumulation of PDGFRα while lysosomal degradation was blocked. After fixation, PDGFRα (R&D Systems, Minneapolis, MN AF 227-NA, 4 μg/ml) and LAMP1 immunostaining (IDB4 5 μg/ml, Developmental Studies Hybridoma Bank, University of Iowa) were visualized by and imaging using a Zeiss LSM710 confocal microscope.

Depletion of APPL1 and APPL2 using small inhibitory-RNA (siRNA). Fibroblasts were isolated from the lungs of TGCre+/-;Nrp1F/- and TGCre+/-;Nrp1F/F mice and cultured in glass-bottom culture dishes (MatTek) for FRET-imaging or in 60 mm dishes for immunoblotting. The effects of APPL1-depletion on PDGFA responsive Akt phosphorylation was assessed using DsiRNA for APPL1 (25 nM mm.Ri.Appl1.13.2 and 25 nM mm.Ri.Appl1.13.3 or 25 nM APPL2 mm.Ri.Appl2.13.1, or a negative control siRNA, NC1 which were purchased from Integrated DNA Technologies (IDT, Coralville, IA).

Preliminary experiments established that these concentrations reduced APPL1 by approximately 65% and APPL2 mRNA by approximately 90%. The siRNA was introduced into LF using TransIT-X2 (Mirus Biotech. Madison, WI) and incubated for 24h. The cultures were then maintained for another 48 h before stimulation with PDGFA to assess Akt-biosensor activity or pS473Akt phosphorylation by immunoblotting.

Quantification of Akt-activity using the AKtAR2 FRET biosensor. Lung fibroblasts which had been isolated from TGCre+/-;Nrp1F/F or littermate control TGCre+/-;Nrp1F/- mice were sub-cultured into glass-bottom dishes (MatTek) and transfected with AktAR2 plasmid using Trans-IT 2020 (Mirus) (12). After culturing the cells for 48 h, FRET imaging was performed following a previously described procedure, except that the exposure time was 1 s, and at least 8 images were captured per condition. Fibroblasts from control mice were transfected with plasmids containing either mCerulean or mVenus, images were captured using conditions identical to those for FRET analysis and were used to calculate the spectral overlap. Images were acquired using the LED light source and filters and were analyzed as previously published, except that cultures of primary LF rather than Mlg2980 cells were used to correct for the spectral overlap (33).

Localization of inositol-3 phosphates in plasma membrane and very early endosomes. The plekstrin-homology domain of Akt (AktPH) which binds inositol phosphorylated at the 3-position of PI(3,4)P2, or PI(3,4,5)P3, was used to determine whether Nrp1 influences the accumulation of these moieties in very early endosomes (15). Lung fibroblasts isolated from TGCre+/-;Nrp1F/- and TGCre+/-;Nrp1F/F were co-transfected with pcDNA3.1-AktPH-GFP and APPL1-mRuby3 and imaged at 37^{o} using TIRF-microscopy, a Nikon CFI APO 60X OIL TIRF NA 1.49 objective at 37^{o}, after exposure to 25 ng/ml PDGFA. The TIRF evanescent field selectively illuminated lamellipodia and VEE which reside within 100 nm of the ventral cell-surface. Excitation intensities and exposure times were held constant and the intensity of GFP emission in regions of interest corresponding to lamellipodia or peripheral VEE were expressed relative to the areas of these respective compartments. After background-subtraction, Fiji (ImageJ2) was

used to systematically threshold the mRuby3 channel to identify endosomal structures that resided outside the perinuclear zone. Lamellipodia were identified by their peripheral location, characteristic shape, and higher intensity of AktPH-eGFP. The intensity of GFP-fluorescence was normalized to the aggregate area of APPL1-containing peripheral vesicles or lamellipodia for each cell.

Western immunoblotting. Lung fibroblasts which had been isolated from TGCre+/-;Nrp1F/F or littermate control TGCre+/-;Nrp1F/- mice were cultured in 60 or100 mm plates. For co-immunoprecipitation of PDGFRα and APPL1, LF were transfected with pCMV-PDGFRα-N-DYKDDDDK and after 48 h the cell layers were washed with PBS, cooled to 4^{o}, and lysed *in situ* in the presence of phosphatase and protease inhibitors (31). The lysate was subjected to immunoprecipitation with Anti-DYKDDDDK (ThermoFisher A36797). To assess the effects of Nrp1-deletion on PDGFRα-signaling, cell layers from a different set of cultures were stimulated with 25 ng/ml PDGFA (R&D Systems) for 20 minutes and then harvested using the same buffer and inhibitors. These cell lysates were clarified by centrifugation, protein was quantified, and the samples were subjected to SDS-PAGE, immunoblotting, and enhanced chemiluminescence-detection (31). The following antibodies were used for detection. PDGFRα: Abcam #ab203491 1:1000; APPL1: Abcam #ab95195 1:10,000; pS473Akt: Cell Signaling #9271, 1:1000; Akt; Cell Signaling #9272, 1:1000; β-tubulin Sigma-Aldrich #T-7816, 1:4000; β-actin: Sigma-Aldrich #A2228 (clone AC-74). The fluorograms were digitally imaged, and the densities were quantified using Fiji (ImageJ2).

Live total internal reflection (TIRF) microscopy. Lung fibroblasts which had been transfected with Nrp1 and PDGFRα were imaged using TIRF-optics to establish that the endocytic vacuoles were positioned within approximately 100 nm from the cell surface (characteristic of very early endosomes). The cells were imaged in the same medium that was used for spinning-disk confocal imaging at 37^{o} and 5% CO_2, which were controlled using a Tokai Hit stage-top incubator. Using a Nikon Ti-E inverted microscope and epifluorescence, cells were selected with approximately the same level of fluorescence intensity for the individual colors (mClover3 and DyLite 543 or GFP and mRuby3) among the cells which were

imaged. This enabled the laser power and exposures time to remain uniform. After tuning the position of the laser beam to achieve TIRF for each color, cells were imaged using a Nikon CFI APO 60X OIL TIRF NA 1.49, which was maintained at 37^{o}. Separate images were captured after successive excitations at 488 and 561 nm including fields lacking cells for background subtraction. After background subtraction the files were exported as Tif format, cropped and merged using Fiji.

Proximity ligation assay. To identify protein interactions among PDGFRα, Nrp1 or APPL1, early endosome antigen-1 (EEA1), GIPC1, or Myo6 we conducted a proximity ligation assay (PLA), which identifies two proteins residing within a 40 nm radius. We used the DuoLink® (Olink Bioscience, Sigma Aldrich St. Louis, MO) kit following the manufacturer's instructions as previously detailed, with the following modifications (31). In some instances, the LF were incubated with PDGFA prior to standard fixation with 4% paraformaldehyde, 5 mM EGTA, 2 mM $MgCl_2$, 80 mM PIPES pH 6.8, to preserve actin filaments (22). Representative experiments analyzing the time course of protein-association of PDGFRα in PLA-granules with Nrp1, EEA1 or APPL1 are shown in Fig. S1 and demonstrate that the associations persist at 20 minutes, when our analyses were timed. The cells were permeabilized with 0.3% triton X-100, blocked with 2% normal donkey serum, and incubated overnight with the primary antibodies which included one from rabbit and another from goat. The primary antibodies used for these studies are shown in supplementary Table 1. To highlight the cytoplasm, F-actin was stained with Acti-stain™ A488 phalloidin (Cytoskeleton, Denver CO) and nuclei with ToPro-3. After imaging with a Zeiss LSM710 confocal microscope, granules were enumerated and classified as peripheral if they were located in lamellipodia, which were devoid of ventral actin fibers or were at the plasma membrane. When actin-transverse arcs were observed they were used to ascertain the base of lamellipodia.

Image processing and analysis. When two genotypes were compared, the cells or lungs from a gene-deleted mouse was compared to its littermate control which did not bear that specific deletion (heterozygous for both TGCre and Nrp1 or PDGFα). Light source intensity, exposure times, and detector gains were optimized at the beginning of the imaging session and were then uniformly applied to all

samples in that imaging session. Confocal images were acquired using the Zeiss LSM 710 or Olympus IX81 at a density of 1024 X 1024 pixels were exported in a BigTif format and then analyzed using Fiji. The color channels were separated and regions of interest (ROI) were drawn and applied to each of the three color-channels to ensure pixel registration across all channels. The periphery of the cell was defined by the outer rim of cortical actin or from the DIC image. Initially, several images representing each genotype were perused and Fiji was used to uniformly subtract background and choose an optimal threshold for each channel, which was applied for that channel to all images that were acquired in a particular imaging session. The intensity of pixels occupied by both fluorescent probes was ascertained and normalized to the intensity of the reference-probe. The "and" command in ROI Manager was used to assess the confluence of areas defined by thresholding and to calculate the intensity for the two different color channels in the region of interest defined by thresholding.

Statistical methods: Box plots with whiskers showing the minimum and maximum and individual points were plotted using GraphPad Prism® (San Diego, CA). "N" is the number of different mice that were used, the number of different experiments that were performed using cell cultures, or individual cells (38). Analysis of variance (either 1 or 2-way as indicated in the figure legends) was performed using Systat (Chicago, IL) or GraphPad Prism® and Student's t-test using Microsoft Excel (either paired or unpaired as indicated in the figure legends). Multiple t-test was performed using GraphPad Prism®. Values of $P < 0.05$ were considered significant.

Results

Summary of our earlier studies which provided the rationale for studying endocytosis of PDGFRα. Using flow cytometry to analyze PDGFRα-expressing LF immediately after isolation, we previously demonstrated that PDGFRα (CD140a) resided intracellularly, as well as on the outer surface and only the latter correlated with Erk1/2-kinase activity (32). Using the same approach, we confirmed these findings with LF isolated from TGCre+/-;Nrp1F/- and TGCre+/-;Nrp1F/F littermates for which 88.92 ± 0.03 and

89.44 ± 0.04% respectively (mean ± SD, n=5) of CD140a was located intracellularly. We previously showed that after stimulation with PDGFA, cell-surface Nrp1 and PDGFRα coordinately enter the cell (34). These findings suggest that PDGFRα signaling may differ by location and prompted our current investigations of intracellular signaling by PDGFRα.

Entry of PDGFRα into early (sorting) endosomes is regulated by Nrp1. We sought to identify the intracellular compartment(s) into which PDGFRα and Nrp1 enter. In LF isolated from wildtype mice, PDGFA promoted the accumulation of PDGFα and Nrp1 in cytoplasmic granules which also contained EEA1 (Fig. 1A). We used the proximity ligation assay (PLA) to quantify colocalization. Two secondary antibodies conjugated to two different oligonucleotides, which upon annealing identify contiguous antigen-antibody complexes, allowed us to colocalize PDGFRα and EEA1 within a 40 nm radius. This falls below the diffraction limit of light microscopy, but the locations are identified because amplification of the nucleotide-duplex provides a visible fluorescent granule. We observed that a 20-minute exposure to PDGFA produced a greater than 10-fold increase in PDGFRα colocalization with EEA1 in LF from TGCre+/-;Nrp1F/- mice, which was significantly reduced in LF isolated from TGCre+/-;Nrp1F/F littermates (Fig. 1B). . Therefore neuropilin-1 both co-localized with and regulates the accumulation of PDGFRα in EEA1+ sorting endosomes. Figure S1 shows that PDGFRα remained associated with Nrp1 (A) or APPL1 (B) for more than 20 minutes. Panel C shows absence of PLA granules using non-immune IgG, verifying the specificity of the primary antibodies. Figure S1 panels D-F show that when non-immune IgG was used in lieu of primary antibodies, very few granules were observed.

Entry of PDGFRα into signaling (very early) endosomes is regulated by Nrp1. The small GTPase Rab5 is found in both sorting (EEA1-containing) and signaling (APPL1-containing, very early) endosomes (10). Because the kinase activity of RTKs is retained in signaling endosomes (VEE), Nrp1 could enhance PDGFA-mediated signaling by directing PDGFRα to VEEs. Therefore, we used the PLA to assess the colocalization of PDGFRα and APPL1. We observed that PDGFA increased the association of PDGFRα and APPL1 which was significantly lower in LF from TGCre+/-;Nrp1F/F compared to LF from littermate

control TGCre+/-;Nrp1 F/- mice (Fig. 2A and B). Using anti-PDGFRα to probe cell-lysates following stimulation of LF with PDGFA, we observed co-immunoprecipitation of PDGFRα and APPL1, which was less abundant in LF from TGCre+/-;Nrp1F/F mice (Fig. 2C and D).

Because the PDGFA ligand was presented extracellularly, cell-surface PDGFRα was instrumental in augmenting the colocalization with APPL1. However, the PLA detected PDGFRα molecules which were already associated with APPL1, as well as receptors that had been endocytosed only after PDGFA-stimulation. To further assess the trafficking of newly endocytosed PDGFRα, we used the "antibody feeding assay" to specifically probe the trafficking of cell-surface PDGFRα. The LF were maintained at 4^{o} permitting anti-DYKDDDDK to bind only to the exteriorized N-terminal PDGFRα-DYKDDDDK, and after warming to 37^{o} live-cell imaging was used to quantify the colocalization of PDGFRα-DYKDDDDK:anti-DYKDDDDK with RAb5- or APPL1-containing vesicles. For this analysis we limited quantification to cytoplasmic granules that resided more peripherally than the perinuclear zone, to exclude the region where most of the lysosomes resided. Representative DIC images showing the location of Rab5 or Rab7 containing structures demonstrate that whereas Rab7 is only observed in the perinuclear region, Rab5 is also located more peripherally (Fig S2). Although we optimized transfections to limit expression of the recombinant DYKDDDDK and mRuby3 fusion proteins, a significant portion of both accumulated in lysosomes. Colocalization in lysosomes would reflect terminal processing of the recombinant proteins and may not inform whether PDGFRα and APPL1 co-localized before reaching lysosomes. After stimulation with PDGFA, more PDGFRα (intensity of Dylite 543 fluorescence) was observed in pixels which contained Rab5 in LF from TGCre+/-;Nrp1F/- mice compared to those from their TGCre+/-;Nrp1F/F littermates (Fig. 3A and B).

Because Rab5 is present in both sorting and very early endosomes, we used the "antibody feeding assay" to assess colocalization of PDGFRα with APPL1, which is limited to signaling endosomes. As we observed for Rab5, Nrp1-deletion significantly reduced the intensity of PDGFRα-DYKDDDDK fluorescence that co-localized with APPL1-containing vesicles (Fig. 3C and D). Total internal reflection

328 microscopy (TIRF-M) limits the depth of fluorescence illumination to the 100 nm closest to the glass
329 coverslide and has been used to visualize VEE (54). Using TIRF-illumination, we observed
330 colocalization of PDGFRα and APPL1 within the 100 nm penetration of the evanescent wave, supporting
331 their presence in very early (signaling) endosomes (Fig. 3E). In LF from controls (left panel) more
332 peripheral granules are yellow, indicating colocalization of APPL1 and PDGFRα, whereas fewer were
333 observed in LF with depleted Nrp1 (right). Therefore, Nrp1 promoted the accumulation of PDGFRα in
334 VEE where it may retain its kinase activity.

335 Using the PLA for wildtype LF, we observed that, as for PDGFRα, PDGFA increased association
336 between Nrp1 and APPL1 (Fig. 4A and B). The "antibody feeding assay" was also used to colocalize
337 transfected Nrp1-mClover3 and APPL1-mRuby3 (Fig. 4C). We observed that more than 50% of the
338 Nrp1 in peripheral granules was located where APPL1 also resided. However, colocalization of Nrp1 and
339 APPL1 was not altered by PDGFRα-deletion. These findings indicate that Nrp1 accompanies PDGFRα
340 upon entry into APPL1-containing signaling endosomes, but that PDGFRα is not required for Nrp1 to
341 enter signaling endosomes.

342 *Association of the Nrp1 binding-partner GIPC1 with myosin 6 is altered by Nrp1-depletion*. APPL1
343 forms homodimers or heterodimerizes with APPL2, enabling the two phospho-tyrosine-binding (PTB)-
344 domains to bind different cargos (9). Both Nrp1 and APPL1 can associate with GIPC1, which is also a
345 binding partner for Myo6 (50). The (PTB) of APPL1 interacts with phosphorylated RTKs such as the
346 insulin-receptor, thereby tethering them to GIPC1, which binds to the carboxy-terminal domain of APPL1
347 (9). We next used the PLA to assess whether Nrp1 influences the ability of Myosin 6 to load cargo which
348 is tethered to GIPC. Exposure to PDGFA increased associations between GIPC1 and Myo6 in LF
349 isolated from TGCre+/-;Nrp1F/- but not TGCre+/-;Nrp1F/F, suggesting that Np1 enhanced the loading of
350 signaling endosomes onto Myo6 (Fig. 4D).

351 *Entry of PDGFRα into the late endosomal pathway is also regulated by Nrp1*. To further evaluate the
352 trafficking of endosomal PDGFRα we also assessed accumulation in late endosomes. Using the

353 "antibody feeding assay" to co-localized PDGFRα with the late-endosomal marker Rab7, we observed
354 that Nrp1-depletion reduced the fraction of recently internalized PDGFRα that co-localized with Rab7
355 after exposure to PDGFA (Fig. 5A). Representative images are shown in Fig. S3. Using leupeptin to
356 minimize lysosomal proteolysis and allow late-endosomal PDGFRα to accumulate, we observed that
357 Nrp1-depletion decreased immunoreactive PDGFRα that co-localized to early endosomes, and into the
358 degradative pathway (Fig. 5B). Representative images are shown in Fig. S4. This indicates that Nrp1
359 increased the overall endocytic flux of PDGFRα.

360 *Nrp1 and APPL1 promote PDGFA activated signaling by PDGFRα through Akt*. The
361 phosphatidylinositol 3-kinase (PI3K)/Akt pathway is a major downstream signaling conduit for PDGFRα
362 in mouse LF, and APPL1 directly interacts with Akt (9). Therefore, we evaluated Akt-activity and
363 phosphorylation in LF with genetically-depleted Nrp1 first without depletion of APPL1. Following
364 stimulation with PDGFA, immunoblotting demonstrated that the phosphorylation of Akt on S^{473} was
365 lower from TGCre+/-;Nrp1F/F mice compared to those from TGCre+/-;Nrp1F/- littermates (Fig. 6A, B).
366 A similar observation was made using the AktAR2 Förster resonance energy transfer (FRET) biosensor
367 which quantifies the activity of Akt by its ability to engage its substrate domain with the Akt binding site
368 of FoxO1 (Fig. 6C).

369 The plekstrin homology (PH)-domain of Akt folds onto its kinase domain to maintain latency in the
370 absence of PI(3,4)P2 or PI(3,4,5)P3 (14). Conversely when the PH-domain binds one of these PI(3)P
371 moieties, Akt is activated. Therefore, the intensity of AktPH-GFP informs about the location and
372 activation state of Akt (52). We used AktPH-GFP to determine whether active Akt-kinase localizes to
373 APPL1-containing VEE, and whether Nrp1 increases localization (Fig. 6D). Whereas lamellipodia-
374 associated AktPH was independent of Nrp1, Nrp1-depleted LF exhibited significantly less active Akt in
375 APPL1 containing endosomal vesicles (Fig. 6E). Representative cells showing AktPH-GFP in the
376 absence and presence of PDGFA and lamellipodial AktPH-GFP in the membrane are shown in Figure S6.

377 We then used the AktAR2 biosensor to analyze Akt-activity in regions of the cell containing (VEE) after

APPL1-depletion with siRNA. We observed that, following PDGFA exposure, APPL1-depletion regionally reduced the signaling activity of Akt (Fig. 6 F). Depleting APPL1 reduced AktAR2 biosensor FRET in LF from control TGCre+/-;Nrp1F/- but not those from TGCre+/-;Nrp1F/F mice, further indicating that Nrp1 interacts with APPL1.

We also used immunoblotting to assess pS473Akt phosphorylation in whole cell lysates from cultured LF isolated from either TGCre+/-;Nrp1F/- or TGCre+/-;Nrp1F/F mice were exposed to APPL1 or APPL2 siRNA or a combination. Unlike for AktAR2-FRET and AktPH-eGFP colocalization with APPL1, which analyzed specific regions of the cell, APPL1-depletion did not significantly reduce pS^{473}Akt phosphorylation in immunoblots (Fig. S5). These findings indicate that where PDGFRα, Nrp1 and APPL1 co-localize their interaction increases Akt-kinase activity, but this is not reflected in the global cellular abundance of pS473Akt after exposure to PDGFA.

Discussion

Summary of the major findings. Others observed that PDGFRβ recycles back to the plasma membrane, whereas PDGFRα does not (17). This prompted our query whether PDGFRα-signaling is preserved after internalization into one or more endosomal compartments. Knowing that Nrp1-deletion disrupted secondary alveolar septation, which requires signaling through PDGFRα, we hypothesized that Nrp1 supports PDGFRα entry into and signaling within very early (signaling) and/or early endosomes. A schematic diagram in Figure 7 illustrates the endosomal compartments where we determined that Nrp1 and PDGFRα interact. We observed that Nrp1 gene-deletion reduced the PDGFA induced co-localization of PDGFRα with EEA1 and Rab5, which both mark early endosomes. Using anti-DYKDDDDK to tag exteriorized PDGFRα, after stimulation with PDGFA we observed that PDGFRα co-localized with Nrp1, and that Nrp1-deletion reduced the co-localization of PDGFRα with APPL1. APPL1 is only located in VEE, and was observed using TIRF-illumination, because it resides near the inner plasma membrane and is illuminated by the restricted evanescent field. To our knowledge, this is the first demonstration that

Nrp1 localizes to VEE and that Nrp1 regulates the accumulation of PDGFRα in this endosomal compartment. We also observed that PDGFRα co-localized (PLA and live-imaging) and immunoprecipitated with APPL1, indicating that these proteins closely interact in VEE. These interactions impact PDGFRα-signaling, because PDGFA increased the co-localization of Nrp1 and APPL1 with PDGFRα, and Nrp1-deletion decreased Akt-activity, an important consequence of signaling through PDGFRα. Furthermore, APPL1-depletion decreased PDGFA mediated Akt-activation in membrane compartments where PDGFRα generates PI(3)P, including very early endosomes.

Physical interaction between PDGFRα and APPL1. When the CMV immediate-early promoter was used to express PDGFRα-N-DYKDDDDK, APPL1 co-immunoprecipitated with PDGFRα. It remains uncertain whether PDGFRα directly interacts with APPL1. The phosphotyrosine binding domain (PTB) of APPL1 conforms to a β-sandwich FERM domain which binds pY in the insulin receptor (IR) and insulin receptor substrate (IRS) adapter protein (13). The FERM domain recognizes an amino acid NXXY motif in RTKs such as epithelial growth factor receptor (EGFR), but we could not find a published report indicating that PDGFRα is recognized via this motif (45). Mouse PDGFRα contains the amino acid sequence NGDY, ending at Y^{731} which is a potential PTB-recognition site. Nrp1 contains the amino acid sequence NPEY, which was shown to bind a consensus PxFERM domain in a peptide screen (13). This could indirectly tether PDGFRα to APPL1 through Nrp1. Additional structural studies are required to determine precisely how PDGFRα interacts with Nrp1 and APPL1.

RTK signaling is preserved in very early endosomes. Sequestration of RTK in VEE (signaling endosomes) both preserves and focuses kinase activity close to the inner plasma membrane (16). The endosomal trafficking of the RTKs EGFR and IR has been extensively studied and illustrates how receptor signaling may alternatively be perpetuated or terminated (3). After insulin-binding and autophosphorylation, the IR engages IRS which recruits PI3K to activate Akt. Although these events occur while the IR is still tethered to the plasma membrane, they persist and IR-signaling is enhanced as the signaling-complex transits through Rab5-positive endosomes (3). Following transit of the IR to Rab5-

containing endosomes, APPL1 becomes a critical component of this signaling complex. APPL1 homo- or heterodimerizes with APPL2 conjoining the two PTBs which bind cargo including IRS and Akt (9). The C-terminus of APPL1 binds GIPC which tethers the VEE to Myo6. Although APPL1-containing endosomes were originally thought to be a way station before EEA1-early endosomes, APPL1-containing VEE are now regarded as independent signaling centers (16).

Limitations of our findings. We used three different approaches to examine how APPL1 impacts PDGFRα-signaling through Akt: (a) Showing that of APPL1 resides in endosomes where PI(3,4,5)P3 or PI(3,4)P2 engage the Akt -plekstrin-homology domain (Akt-PH), a requirement for Akt-activation, (b) AktAR2 FRET-imaging which quantified Akt-activation in regions of interest at the periphery of individual cells, and (c) immunoblotting, which analyzed the whole cell lysate pooled from all the cells in a dish. The AktPH-GFP biosensor reports on the abundance of PI(3,4)P2 and PI(3,4,5)P3 which designates but does not directly assess Akt-activation, as is the case with immunoblotting. But immunoblotting could not assess specific interactions between endosomal APPL1 and Akt, because not all Akt resides in APPL1-containing endosomes. Nrp1-depletion altered the accumulation of AktPH-GFP in VEE but not in lamellipodia where PI(3,4,5)P3 dominates, and APPL1 and 2 knock down did not significantly reduce whole cell pS^{473}Akt. Although Nrp1 enhances PDGFRα-mediated Akt-activation in LF, the requirement for APPL1 and -2 is limited to signaling in VEE where APPL1 and -2 reside. During murine embryonic development and in cultured LF, PI3K-Akt is the major downstream signaling pathway that is initiated by PDGFRα-phosphorylation (18) (30) (32). To assess how Nrp1 promotes PDGFRα signaling, we focused on the activation of Akt because this is the dominant pathway and is most likely to influence LF functions including proliferation, survival, and migration (30) (33). It is clear that Akt directly interacts with APPL1, but our studies do not exclude interactions between Nrp1 and other downstream signaling intermediates which may also enhance PDGFRα-signaling (9).

Our findings do not establish that APPL1 or -2 are required for PDGFRα signaling in the lung. Although hepatocyte growth factor-mediated Akt phosphorylation was reduced in embryonic fibroblasts from mice

with combined deletion of both APPL1 and APPL2, no obvious pulmonary developmental defects were observed (48). Despite these limitations, we have made novel observations that Nrp1 and PDGFA promote physiologically relevant associations between PDGFRα and APPL1, via a pathway involving VEE.

How very early endosomes may enhance PDGFRα-signaling. There are several mechanisms whereby guiding PDGFRα to VEEs may increase signaling. (a) Although PDGFRα phosphorylates and activates PI3K at the plasma membrane to generate phosphatidylinositol tris-phosphate PI(3,4,5)P3, this is dephosphorylated by membrane-associated phosphatase and tensin homolog (PTEN) (46). Entry into endosomal vesicles, sequesters PI(3,4,5)P3 from PTEN. Phosphatidylinositol 3,4-bisphosphate PI(3,4)P2 can be generated from PI(3,4,5)P3 at the plasma membrane or in vesicles, where it activates Akt2, which being exclusively endosomal, is sequestered from plasma membrane-associated protein phosphatase-2 (PP2A). (b) Tethering PDGFRα in VEEs holds it in the submembrane space where it may engage Myo6 for positioning where lamellipodia and filopodia are generated (27). (c) Maintenance in VEEs suspends transport of PDGFRα to multivesicular bodies and ultimately lysosomes, where it would be degraded. Additional mechanisms for preserving PDGFRα-signaling have been proposed and may also sustain PDGFRα-signaling (7) (35) (43).

How Nrp1 guides proteins into VEE. APPL1 regulates the density of β1-integrins at the leading edge of migrating cells, thereby influencing focal adhesion formation and migration velocity (8) (20). Valdembri and associates showed that by interacting with the APPL1-binding partner GIPC1, Nrp1 enhances β1-integrin recycling and adhesion of endothelial cells to fibronectin (51). The carboxy-terminal SEA domain of Nrp1 was required, in coordination with GIPC1 and Myo6, to recycle integrin-α5 back to the plasma membrane; and integrin-α5 and Nrp1 co-localized in vesicles below and on the plasma membrane. They proposed that Nrp1 may guide α5β1 integrin to an endosomal compartment, where APPL1 tethers α5β1 to GIPC1 and Myo6 for return to the cell surface.

VEE enhance lamellipodia formation. Migrating fibroblasts polarize so lamellipodia reside at the

leading-edge during migration. Lamellipodia are highly dynamic structures where branched actin filaments form and remodel as the cell probes its environment and extends forward. We have previously shown that Rac1 is a downstream intermediate of PDGFRα-signaling, which is required for LF to respond to rigidity (durotaxis) and migrate on collagen fibers (33). Polarization involves preferential generation of Rac1-GTP at the leading edge as Rac1 and Rac1-guanine exchange factors (GEF)s associate with membrane structures in lamellipodia (47). Phosphoinositides including PI(3,4,5)P3 and PI(3,4)P2 are generated at membranes and recruit Rac-GEFs, which in turn promote PI3K activity (6). Endosomal vesicles provide a portable source of lipids, which can be recruited to the leading edge. Here they support Rac1-GEF recruitment, generation of Rac1, and activation of the Wiskott-Aldrich syndrome protein family verprolin homolog (WAVE) complex, and may preserve PI(3,4,5)P3 precisely where lamellipodial branched actin forms (42). Therefore, at the leading edge APPL1-containing VEEs may be a geographically positioned, readily recruitable, activated platform promoting lamellipodial actin remodeling by PDGFRα.

Sustained PDGFα-signaling in pulmonary development and disease. Our findings are relevant to bronchopulmonary dysplasia (BPD), emphysema and pulmonary fibrosis. Whereas PDGFRα was originally proposed to expand and relocate alveolar septal myofibroblast progenitors (5) (25), a more recent study using postnatally induced targeted depletion in septal myofibroblasts, showed that sustained PDGFRα signaling establishes the elastogenic phenotype and enhances the expression of genes required for myofibroblast migration (23). In a model of BPD, postnatal hyperoxia induced miR34a, which in turn decreased PDGFRα gene expression and disrupted alveolarization (39). These changes were reversed by an oligonucleotide which specifically disrupted miR34a-PDGFRα interactions. Therefore, sustained expression of PDGFRα is required for alveolarization and postnatal disruption contributes to BPD. Further support comes from studies of mechanically ventilated premature infants who subsequently developed BPD and were compared to a ventilated cohort who did not develop BPD (11). Mesenchymal cells lavaged from the lungs of the BPD cohort expressed less PDGFRα, which was accompanied by

reduced expression of genes involved in pathways which are regulated by PDGFRα, including cell proliferation and motility. Our findings provide a potential mechanism whereby alveolar myofibroblasts sustain intracellular PDGRα signaling to enhance septation.

Our findings are also relevant to diseased lungs in adults. Gene expression analysis using lung tissues from cross-sectional cohorts of humans with emphysema, idiopathic pulmonary fibrosis (IPF), and controls without lung disease demonstrated that the shorter splice-variant of PDGFA was relatively more abundant in diseased subjects (19). The shorter splice variant in both mice and humans has a terminal arginine (R), whereas the longer variant, which includes exon 6, ends with a heparin binding motif. The terminal R is part of the CendR motif in VEGF-165 which is required for binding to the b-domain of Nrp1(49). This interaction has been intensely studied and has fostered the development of tumor-penetrating peptides which take advantage of surface molecules such as integrin α5, which are overexpressed on tumor cells (40) (49). These peptides contain an integrin binding motif to target cancer cells, conjoined to a CendR motif and a cargo chemotherapeutic agent and ensure preferential delivery of the agent to cancer cells (41). Observing that Nrp1 interacts with PDGFRα, the sole receptor for PDGFAA, raises the tantalizing possibility that Nrp1 and the terminal R on the short form of PDGFA, which is over-represented in emphysema and IPF could be leveraged to target drug delivery to important effector cells in these diseases. Using adult mice with fibrotic lungs, others have shown that PDGFRα-expressing pulmonary mesenchymal cells have a distinct lineage and exhibit a characteristic gene-expression profile for fibrillar collagen, further supporting a role for these cells in pulmonary fibrosis (4). Because gene-expression profiling of the PDGFRα-expressing population may vary between neonates and adults, further investigations using LF from adults are required.

Acknowledgment

The studies were supported by Merit Review and shared equipment grants from the Department of Veterans Affairs Research Service.

References

1. **Amy RM, Bowes D, Burri PH, Haines J and Thurlbeck WM**. Postnatal growth of the mouse lung. *J Anat* 124: 131-151, 1977.
2. **Ball SG, Bayley C, Shuttleworth CA and Kielty CM**. Neuropilin-1 regulates platelet-derived growth factor receptor signalling in mesenchymal stem cells. *Biochem J* 427: 29-40, 2010.
3. **Bergeron JJ, Di Guglielmo GM, Dahan S, Dominguez M and Posner BI**. Spatial and Temporal Regulation of Receptor Tyrosine Kinase Activation and Intracellular Signal Transduction. *Annu Rev Biochem* 85: 573-597, 2016.
4. **Biasin V, Crnkovic S, Sahu-Osen A, Birnhuber A, El AE, Sinn K, Klepetko W, Olschewski A, Bellusci S, Marsh LM and Kwapiszewska G**. PDGFRalpha and alphaSMA mark two distinct mesenchymal cell populations involved in parenchymal and vascular remodeling in pulmonary fibrosis. *Am J Physiol Lung Cell Mol Physiol* 2020.
5. **Boström H, Willetts K, Pekny M, Leveen P, Lindahl P, Hedstrand H, Pekna M, Hellstrom M, Gebre-Medin S, Schalling M, Nilsson M, Kurland S, Tornell J, Heath JK and Betsholtz C**. PGDF-A signaling is a critical event in lung alveolar myofibroblast development and alveogenesis. *Cell* 85: 863-873, 1996.
6. **Cao X, Kaneko T, Li JS, Liu AD, Voss C and Li SS**. A phosphorylation switch controls the spatiotemporal activation of Rho GTPases in directional cell migration. *Nat Commun* 6: 7721, 2015.
7. **Clement DL, Mally S, Stock C, Lethan M, Satir P, Schwab A, Pedersen SF and Christensen ST**. PDGFRα signaling in the primary cilium regulates NHE1-dependent fibroblast migration via coordinated differential activity of MEK1/2-ERK1/2-p90RSK and AKT signaling pathways. *J Cell Sci* 126: 953-965, 2013.
8. **Diggins NL, Kang H, Weaver A and Webb DJ**. alpha5beta1 integrin trafficking and Rac activation are regulated by APPL1 in a Rab5-dependent manner to inhibit cell migration. *J Cell Sci* 131: 1-18, 2018.

9. **Diggins NL and Webb DJ**. APPL1 is a multifunctional endosomal signaling adaptor protein. *Biochem Soc Trans* 45: 771-779, 2017.
10. **Donaldson JG, Johnson DL and Dutta D**. Rab and Arf G proteins in endosomal trafficking and cell surface homeostasis. *Small GTPases* 7: 247-251, 2016.
11. **Fulton CT, Cui TX, Goldsmith AM, Bermick J and Popova AP**. Gene Expression Signatures Point to a Male Sex-Specific Lung Mesenchymal Cell PDGF Receptor Signaling Defect in Infants Developing Bronchopulmonary Dysplasia. *Sci Rep* 8: 17070, 2018.
12. **Gao X and Zhang J**. Spatiotemporal analysis of differential Akt regulation in plasma membrane microdomains. *Mol Biol Cell* 19: 4366-4373, 2008.
13. **Ghai R, Bugarcic A, Liu H, Norwood SJ, Skeldal S, Coulson EJ, Li SS, Teasdale RD and Collins BM**. Structural basis for endosomal trafficking of diverse transmembrane cargos by PX-FERM proteins. *Proc Natl Acad Sci U S A* 110: E643-E652, 2013.
14. **Hawkins PT and Stephens LR**. Emerging evidence of signalling roles for PI(3,4)P2 in Class I and II PI3K-regulated pathways. *Biochem Soc Trans* 44: 307-314, 2016.
15. **Johnson HE and Haugh JM**. Quantitative analysis of phosphoinositide 3-kinase (PI3K) signaling using live-cell total internal reflection fluorescence (TIRF) microscopy. *Curr Protoc Cell Biol* 61: 14, 2013.
16. **Kalaidzidis I, Miaczynska M, Brewinska-Olchowik M, Hupalowska A, Ferguson C, Parton RG, Kalaidzidis Y and Zerial M**. APPL endosomes are not obligatory endocytic intermediates but act as stable cargo-sorting compartments. *J Cell Biol* 211: 123-144, 2015.
17. **Karlsson S, Kowanetz K, Sandin A, Persson C, Ostman A, Heldin CH and Hellberg C**. Loss of T-cell protein tyrosine phosphatase induces recycling of the platelet-derived growth factor (PDGF) beta-receptor but not the PDGF alpha-receptor. *Mol Biol Cell* 17: 4846-4855, 2006.
18. **Klinghoffer RA, Hamilton TG, Hoch R and Soriano P**. An allelic series at the PDGFalphaR locus indicates unequal contributions of distinct signaling pathways during development. *Dev Cell* 2: 103-113, 2002.

19. **Kusko RL, Brothers JF, Tedrow J, Pandit K, Huleihel L, Perdomo C, Liu G, Juan-Guardela B, Kass D, Zhang S, Lenburg M, Martinez F, Quackenbush J, Sciurba F, Limper A, Geraci M, Yang I, Schwartz DA, Beane J, Spira A and Kaminski N**. Integrated Genomics Reveals Convergent Transcriptomic Networks Underlying Chronic Obstructive Pulmonary Disease and Idiopathic Pulmonary Fibrosis. *Am J Respir Crit Care Med* 194: 948-960, 2016.

20. **Lakoduk AM, Roudot P, Mettlen M, Grossman HM, Schmid SL and Chen PH**. Mutant p53 amplifies a dynamin-1/APPL1 endosome feedback loop that regulates recycling and migration. *J Cell Biol* 218: 1928-1942, 2019.

21. **Leslie KO, Mitchell JJ, Woodcock-Mitchell JL and Low RB**. Alpha smooth muscle actin expression in developing and adult human lung. *Differentiation* 44: 143-149, 1990.

22. **Leyton-Puig D, Kedziora KM, Isogai T, van den Broek B, Jalink K and Innocenti M**. PFA fixation enables artifact-free super-resolution imaging of the actin cytoskeleton and associated proteins. *Biol Open* 5: 1001-1009, 2016.

23. **Li C, Lee MK, Gao F, Webster S, Di H, Duan J, Yang CY, Bhopal N, Peinado N, Pryhuber G, Smith SM, Borok Z, Bellusci S and Minoo P**. Secondary crest myofibroblast PDGFRalpha controls the elastogenesis pathway via a secondary tier of signaling networks during alveologenesis. *Development* 146: 2019.

24. **Li C, Li M, Li S, Xing Y, Yang CY, Li A, Borok Z, De LS and Minoo P**. Progenitors of Secondary Crest Myofibroblasts are Developmentally Committed in Early Lung Mesoderm. *Stem Cells* 33: 999-1012, 2014.

25. **Lindahl P, Karlsson L, Helstrom M, Gebre-Medhin S, Willetts K, Heath JK and Betsholtz C**. Alveogenesis failure in PDGF-A-deficient mice is coupled to lack of distal spreading of alveolar smooth muscle cell progenitors during lung development. *Development* 124: 3943-3953, 1997.

26. **Mahmoud M, Evans IM, Mehta V, Pellet-Many C, Paliashvili K and Zachary I**. Smooth muscle cell-specific knockout of neuropilin-1 impairs postnatal lung development and pathological vascular smooth muscle cell accumulation. *Am J Physiol Cell Physiol* 316: C424-C433, 2019.

27. **Masters TA and Buss F**. Filopodia formation and endosome clustering induced by mutant plus-end-directed myosin VI. *Proc Natl Acad Sci U S A* 114: 1595-1600, 2017.
28. **Masters TA, Tumbarello DA, Chibalina MV and Buss F**. MYO6 Regulates Spatial Organization of Signaling Endosomes Driving AKT Activation and Actin Dynamics. *Cell Rep* 19: 2088-2101, 2017.
29. **McGowan SE, Grossmann RE, Kimani PW and Holmes AJ**. Platelet-derived growth factor receptor-alpha-expressing cells localize to the alveolar entry ring and have characteristics of myofibroblasts during pulmonary alveolar septal formation. *Anat Rec* 291: 1649-1661, 2008.
30. **McGowan SE and McCoy DM**. Fibroblasts expressing PDGF-receptor-alpha diminish during alveolar septal thinning in mice. *Pediatr Res* 70: 44-49, 2011.
31. **McGowan SE and McCoy DM**. Regulation of fibroblast lipid storage and myofibroblast phenotypes during alveolar septation in mice. *Am J Physiol Lung Cell Mol Physiol* 307: L618-L631, 2014.
32. **McGowan SE and McCoy DM**. Fibroblast growth factor signaling in myofibroblasts differs from lipofibroblasts during alveolar septation in mice. *Am J Physiol Lung Cell Mol Physiol* 309: L463-L474, 2015.
33. **McGowan SE and McCoy DM**. Platelet-derived growth factor receptor-alpha (PDGFRalpha) and Ras-related C3 botulinum toxin substrate-1 (Rac1) regulate mechano-responsiveness of lung fibroblasts. *Am J Physiol Lung Cell Mol Physiol* 313: L1174-L1187, 2017.
34. **McGowan SE and McCoy DM**. Neuropilin-1 and platelet-derived growth factor receptors cooperatively regulate intermediate filaments and mesenchymal cell migration during alveolar septation. *Am J Physiol Lung Cell Mol Physiol* 315: L102-L115, 2018.
35. **Noda K, Kitami M, Kitami K, Kaku M and Komatsu Y**. Canonical and noncanonical intraflagellar transport regulates craniofacial skeletal development. *Proc Natl Acad Sci U S A* 113: E2589-E2597, 2016.

36. **Pellet-Many C, Frankel P, Evans IM, Herzog B, Junemann-Ramirez M and Zachary IC**. Neuropilin-1 mediates PDGF stimulation of vascular smooth muscle cell migration and signalling via p130Cas. *Biochem J* 435: 609-618, 2011.

37. **Rizzolio S and Tamagnone L**. Antibody-Feeding Assay: A Method to Track the Internalization of Neuropilin-1 and Other Cell Surface Receptors. *Methods Mol Biol* 1493: 311-319, 2017.

38. **Rosner B**. *Fundamentals of Biostatistics*. Boston: PWS-Kent Publishing Co., 1990.

39. **Ruiz-Camp J, Quantius J, Lignelli E, Arndt PF, Palumbo F, Nardiello C, Surate Solaligue DE, Sakkas E, Mizikova I, Rodriguez-Castillo JA, Vadasz I, Richardson WD, Ahlbrecht K, Herold S, Seeger W and Morty RE**. Targeting miR-34a/Pdgfra interactions partially corrects alveologenesis in experimental bronchopulmonary dysplasia. *EMBO Mol Med* 11: e9448, 2019.

40. **Ruoslahti E**. Tumor penetrating peptides for improved drug delivery. *Adv Drug Deliv Rev* 110-111: 3-12, 2017.

41. **Saalik P, Lingasamy P, Toome K, Mastandrea I, Rousso-Noori L, Tobi A, Simon-Gracia L, Hunt H, Paiste P, Kotamraju VR, Bergers G, Asser T, Ratsep T, Ruoslahti E, Bjerkvig R, Friedmann-Morvinski D and Teesalu T**. Peptide-guided nanoparticles for glioblastoma targeting. *J Control Release* 308: 109-118, 2019.

42. **Schaks M, Singh SP, Kage F, Thomason P, Klunemann T, Steffen A, Blankenfeldt W, Stradal TE, Insall RH and Rottner K**. Distinct Interaction Sites of Rac GTPase with WAVE Regulatory Complex Have Non-redundant Functions in Vivo. *Curr Biol* 28: 3674-3684, 2018.

43. **Schmid FM, Schou KB, Vilhelm MJ, Holm MS, Breslin L, Farinelli P, Larsen LA, Andersen JS, Pedersen LB and Christensen ST**. IFT20 modulates ciliary PDGFRalpha signaling by regulating the stability of Cbl E3 ubiquitin ligases. *J Cell Biol* 217: 151-161, 2018.

44. **Sheehan P and Waites CL**. Coordination of synaptic vesicle trafficking and turnover by the Rab35 signaling network. *Small GTPases* 10: 54-63, 2019.

45. **Smith MJ, Hardy WR, Murphy JM, Jones N and Pawson T**. Screening for PTB domain binding partners and ligand specificity using proteome-derived NPXY peptide arrays. *Mol Cell Biol* 26: 8461-8474, 2006.
46. **Sugiyama MG, Fairn GD and Antonescu CN**. Akt-ing Up Just About Everywhere: Compartment-Specific Akt Activation and Function in Receptor Tyrosine Kinase Signaling. *Front Cell Dev Biol* 7: 70, 2019.
47. **Takahashi M, Rikitake Y, Nagamatsu Y, Hara T, Ikeda W, Hirata K and Takai Y**. Sequential activation of Rap1 and Rac1 small G proteins by PDGF locally at leading edges of NIH3T3 cells. *Genes Cells* 13: 549-569, 2008.
48. **Tan Y, Xin X, Coffey FJ, Wiest DL, Dong LQ and Testa JR**. Appl1 and Appl2 are Expendable for Mouse Development But Are Essential for HGF-Induced Akt Activation and Migration in Mouse Embryonic Fibroblasts. *J Cell Physiol* 231: 1142-1150, 2016.
49. **Teesalu T, Sugahara KN, Kotamraju VR and Ruoslahti E**. C-end rule peptides mediate neuropilin-1-dependent cell, vascular, and tissue penetration. *Proc Natl Acad Sci U S A* 106: 16157-16162, 2009.
50. **Tumbarello DA, Kendrick-Jones J and Buss F**. Myosin VI and its cargo adaptors - linking endocytosis and autophagy. *J Cell Sci* 126: 2561-2570, 2013.
51. **Valdembri D, Caswell PT, Anderson KI, Schwarz JP, Konig I, Astanina E, Caccavari F, Norman JC, Humphries MJ, Bussolino F and Serini G**. Neuropilin-1/GIPC1 signaling regulates alpha5beta1 integrin traffic and function in endothelial cells. *PLoS Biol* 7: e25, 2009.
52. **Weiger MC, Wang CC, Krajcovic M, Melvin AT, Rhoden JJ and Haugh JM**. Spontaneous phosphoinositide 3-kinase signaling dynamics drive spreading and random migration of fibroblasts. *J Cell Sci* 122: 313-323, 2009.
53. **Zachary I**. Neuropilins: Role in signaling, angiogenesis, and disease. *Chem Immunol Allergy* 99: 37-70, 2014.

54. **Zoncu R, Perera RM, Balkin DM, Pirruccello M, Toomre D and De CP**. A phosphoinositide switch controls the maturation and signaling properties of APPL endosomes. *Cell* 136: 1110-1121, 2009.

682 **Figure Legends**

683 **Figure 1**: *Platelet-derived growth factor receptor-α (PDGFRα) and Neuropilin-1 (Nrp1) colocalize to*
684 *early endosomes*. Lung fibroblasts (LF) were isolated at postnatal day (P)12 from wildtype mice, or from
685 TGCre+/-;Nrp1F/F and their TGCre+/-;Nrp1F/- littermate controls and cultured on glass which had been
686 coated with fibronectin. Prior to fixation, some cultures were exposed to PDGFA for 20 minutes.
687 Immunostaining was performed (A) to detect early endosome antigen-1 (EEA1, blue), neuropilin-1
688 (Nrp1) (green) and platelet-derived growth factor receptor-alpha (PDGFRα, red) and images were
689 acquired using a Zeiss LSM710 laser scanning confocal microscope. Inset shows staining in absence of
690 primary antibodies (non-immune IgG). Staining and imaging sessions always analyzed LF from
691 littermate pairs which were processed and analyzed under identical conditions. Colocalization was
692 observed more frequently (arrows) after exposure to PDGFA. The proximity ligation assay (PLA) was
693 used to compare colocalization (quantity of granules representing presence of two antigens within a 40
694 nm radius) of PDGFRα and early antigen-1 (EEA1) in LF obtained from TGCre+/-;Nrp1F/F and their
695 TGCre+/-;Nrp1F/- littermate controls (B). Ordinate scale: quantity of PLA granules per PDGFA exposed
696 cell normalized to the mean for unexposed LF in that staining session. Cells analyzed for each condition:
697 TGCre+/-;Nrp1F/- no PDGFA and + PDGFA 68 and 72, respectively; TGCre+/-;Nrp1F/F no PDGFA
698 and + PDGFA 80 and 90, respectively. Box and whisker (minimum to maximum, min to max) plots of
699 data pooled from 4 separate cell isolations, in which the data are expressed relative to TGCre+/-;Nrp1F/-
700 no PDGFA condition, 2-way ANOVA. P-values are shown with brackets.

701 **Figure 2**: *PDGFRα resides in signaling endosomes and Nrp1 increased colocalization with adaptor*
702 *protein containing a pleckstrin homology domain and a phosphotyrosine-binding domain-1 (APPL1)*. LF
703 from TGCre+/-;Nrp1F/F and TGCre+/-;Nrp1F/- littermates were isolated and cultured as in Fig. 1, and
704 the PLA was performed to assess colocalization of PDGFRα and APPL1. Representative Zeiss LSM710
705 confocal microscopic fields are shown for each condition (A). Pseudo-colors for phalloidin-A488
706 stained-actin, granules representing association between PDGFRα and APPL1, and nuclei staining with

ToPro3 are cyan, magenta and yellow, respectively. The quantities of cells analyzed by the PLA for each condition and summarized in (B) were TGCre+/-;Nrp1F/- no PDGFA and + PDGFA 43 and 48, respectively; TGCre+/-;Nrp1F/F no PDGFA and + PDGFA 54 and 64, respectively. Box and whisker (min to max) plots of data pooled from 3 separate cell isolations, and expressed as granules per cell TGCre+/-;Nrp1F/- no PDGFA condition, 2-way ANOVA. Lysates from LF isolated from 5 TGCre+/-;Nrp1F/- and 5 TGCre+/-;Nrp1F/F mice were immunoprecipitated (immpt) with anti-DYKDDDDK and subjected to immunoblotting with anti-PDGFRα, -APPL1, or -βactin. Input shows cell lysates prior to immunoprecipitation. A representative immunoblot is shown (C). Even though all lanes were from the same immunoblot, the optimal exposure for the input samples (left side of line) was shorter than that for the immunoprecipitated samples (right side). The densities of bands for APPL1 in LF from TGCre+/-;Nrp1F/- were compared with those from TGCre+/-;Nrp1F/F without exposure to PDGFA (D, box and whisker, min to max, unpaired t-test).

Figure 3: *Nrp1 regulates accumulation of recently internalized PDGFRα in Rab5- and APPL1-endosomes*. LF from TGCre+/-;Nrp1F/- and TGCre+/-;Nrp1F/F littermates were isolated, transfected with N-DYKDDDDK-PDGFRα and transduced with Baculovirus bearing Rab5-GFP (A) or transfected with both N-DYKDDDDK-PDGFRα and APPL1-mRuby3 (B). After incubating with Dylite-543 (A) or A488-tagged anti- DYKDDDDK at 4^{o}, LF were washed and warmed to 37^{o} to allow internalization. Images of 10 to 12 cells for each treatment group were acquired over 30 minutes after exposure to 25 ng/ml PDGFA using an Olympus IX81 microscope equipped with a spinning disk confocal device (DSU). For each cell, an image was captured using differential interference contrast (DIC) to identify the cell borders and ensure that their viability. Fluorescence images were analyzed using Fiji (NIH-ImageJ2) applying uniform thresholding to assess the intensity of PDGFRα bound to the anti-DYKDDDDK fluorophore. The analysis was limited to peripheral granules to exclude fluorescence accumulation in lysosomes (examples shown at arrows). Representative cells from both genotypes are shown in (A) with Rab5 and PDGFRα pseudo-colored cyan and magenta respectively. The cell outlines are shown in

yellow. Data pooled from 4 separate isolations for which the littermate pairs were transfected, imaged and analyzed in parallel are shown in (B), with dots representing individual cells. Cells analyzed for TGCre+/-;Nrp1F/- and TGCre+/-;Nrp1F/F were 34 and 30, respectively. Box and whisker (min to max) plots, 2-way ANOVA are shown. The intensity of PDGFRα-fluorescence was calculated relative to the intensity of Rab5 in all Rab5-containing peripheral granules (left) or relative to the intensity of Rab5 in only those granules which also contained PDGFRα (right). A similar analysis was used to co-localize PDGFRα and APPL1. Representative cells from both genotypes are shown in (C) with PDGFRα-anti-DYKDDDDK-A488 and APPL1-mRuby3 pseudo-colored cyan and magenta respectively. (D) The intensity of PDGFRα-fluorescence was calculated relative to the intensity of APPL1-containing peripheral granules which also contained APPL1. Twenty-nine cells were analyzed for both TGCre+/-;Nrp1F/- and TGCre+/-;Nrp1F/F littermates pooled from 4 separate isolations. Box and whisker (min to max) plots, 2-way ANOVA are shown. (E) Representative total internal reflection microscopy (TIRF-M) images of LF from TGCre+/-;Nrp1F/- and TGCre+/-;Nrp1F/F littermates demonstrate that PDGFRα-A488 (green) and APPL1-mRuby3 (which only resides intracellularly, red) colocalize (yellow) in peripheral granules immediately (100 nm) beneath the ventral plasma membrane, where most signaling endosomes are located.

Figure 4: PDGFA increases accumulation of *Nrp1 and GIPC1 in APPL1-containing signaling endosomes*. Cultured LF obtained from wildtype mice were incubated for 20 minutes in the presence or absence of PDGFA and analyzed using the PLA to quantify the association of Nrp1 (representative images in A) or GAIP C-terminus-interacting protein (images for GIPC1 are not shown) with APPL1. The granules in 67 and 46 LF (individual dots), pooled from 3 separate isolations, were enumerated to quantify associations between Nrp1 and APPL1, in unexposed and PDGFA-exposed, respectively (B, left). And for analyzing GIPC1 and APPL1, the granules in 102 unexposed and 70 PDGFA-exposed LF pooled from 4 separate isolations were enumerated. Box and whisker (min to max) plots, Student's t-test for unpaired variables (B, right). The colocalization of Nrp1 and APPL1 was also assessed in LF

obtained in 4 different isolations from TGCre+/-;PDGFRαF/- and TGCre+/-;PDGFRαF/F littermates which were co-transfected with Nrp1-mClover3 and APPL1-mRuby3 and imaged using spinning disk confocal microscopy (see legend for Fig. 3). The fraction of Nrp1 in that resides in peripheral granules which also contain APPL1 are shown (C). Box and whisker (min to max) plots of individual cells, 2-way ANOVA are shown (not significantly different). The colocalization of myosin 6 (Myo6) and GIPC1 was assessed in LF obtained in 4 different isolations from TGCre+/-;Nrp1F/- and TGCre+/-;Nrp1F/F littermates using the PLA (D). Cells analyzed for each condition: TGCre+/-;Nrp1F/- no PDGFA and + PDGFA 77 and 66, respectively; TGCre+/-;Nrp1F/F no PDGFA and + PDGFA 74 and 92, respectively. Box and whisker (min to max) plots of data pooled from all 4 isolations, in which the data are expressed relative to TGCre+/-;Nrp1F/- no PDGFA condition, 2-way ANOVA.

Figure 5: *Neuropilin-1 regulates entry of PDGFRα into late endosomes*. PDGFRα was co-localized with late endosomal marker Rab7 or LAMP1in LF isolated from TGCre+/-:Nrp1F/- with TGCre+/-;Nrp1F/F. The cells were transfected with N-DYKDDDDK-PDGFRα (see Fig. 2 legend) and then transduced with Baculovirus bearing Rab7-RFP. After incubation with anti-DYKDDDDK-Dy543, the cells were exposed to 25 ng/ml PDGFA, warmed to 37^{o}, and imaged over 30 minutes. Images were acquired from 29 and 30 LF pooled from 3 separate isolations for TGCre+/-;Nrp1F/- and TGCre+/-;Nrp1F/F mice, respectively. Box and whisker (min to max) plots, individual cells, Student's t-test for unpaired variables are shown (A). Lung fibroblasts were isolated from 2 litters of TGCre+/-;Nrp1F/- and TGCre+/-;Nrp1F/F mice and 15 or 21 cells respectively were analyzed to co-localize PDGFRα with the late endosomal marker LAMP1 (B).

Figure 6: *Nrp1 and APPL1 promote signaling by PDGFRα through Akt*. Lung fibroblasts obtained from TGCre+/-;Nrp1F/- and TGCre+/-;Nrp1F/F littermates were cultured and then exposed to 25 ng/ml PDGFA or remained unexposed. Cell lysates harvested in the presence of proteinase and phosphatase inhibitors were subjected to Western immunoblotting probing successively for p473Akt, Akt and βtubulin (βTub). Data were combined from 5 separate experiments, with (**A**) showing a representative

immunoblot. (**B**) Box and whisker (min to max) plots of data pooled from all 5 isolations, 2-way ANOVA. (**C**) Lung fibroblasts isolated from TGCre+/-:Nrp1F/- and TGCre+/-;Nrp1F/F littermates were transfected with an Akt biosensor (AktAR2) and exposed to 50 ng/ml PDGFA and images were acquired for 35 minutes. Y-axis is the mean pixel by pixel ratio for the intensity of the FRET versus the donor channel within all regions of interest (ROI) at the periphery, for a particular cell. Box and whisker (min to max) plots showing individual cells combined from 6 separate cell isolations, with 8 to12 cells per condition, for each isolation. Student's t-test, paired variables. (**D**) LF were co-transfected with AktPH-GFP, which binds to and localizes PI(3,4)P2 and PI(3,4,5)P3 with APPL1-mRuby3, which resides in very early endosomes (VEE). Using TIRF-M to selectively illuminate the plasma membrane and sub-membrane VEE, a uniform thresholding algorithm was applied to identify AktPH-GFP in lamellipodia and in APPL1-containing vesicles. A representative cell with segmented APPL1-containg pixels (red) from a TGCre+/-;Nrp1F/- mouse is shown in (**D**). Mean gray level AktPH-GFP intensity per pixel was compared in regions of interest over APPL1 containing peripheral vesicles or lamellipodia are were compared in LF from TGCre+/-;Nrp1F/- (69 cells) and TGCre+/-;Nrp1F/F(52 cells) mice (left panel, **E**) pooled from 3 mice for each genotype isolated in parallel from 3 different litters. Brackets are box and whisker plots (mean to max), comparisons by multiple t-tests with Bonferroni correction (left panel) and unpaired t-test (right panel). The right panel in E is ratio of the mean intensity over vesicles normalized to that over lamellipodia for each cell. (**F**) Analysis of Akt activity using the AktAR2 FRET-biosensor and protocol described in (C) except that the LF were exposed to APPL1 or negative control siRNA prior to stimulation with 50 ng/ml PDGFA and FRET-imaging. Box and whisker (min to max) plots combining 5 separate cell isolations, with pooled data from 40 cells per condition, 2-way ANOVA.

Figure 7: *Endosomal trafficking of PDGFRα.* At the outer plasma membrane PDGFRα binds PDGFA at lamellipodia (7) in membrane domains shared by Nrp1. After binding PDGFA (diamond) PDGFRα and Nrp1 enter very early (signaling) endosomes (VEE, identified by APPL1, smooth rectangle) and early endosomes (EE, identified by EEA1, hexagon). PDGFRα colocalizes with Nrp1 in both of these

807 compartments and retains kinase activity particularly in VEE (star). PDGFRα can exit EE and move to
808 late endosomes or lysosomes for degradation, but it does not (back slash) enter Rab11- (slow) or Rab4-
809 (fast, not shown) containing recycling endosomes. Very early endosomes are located near the inner
810 plasma membrane, whereas late endosomes and lysosomes are perinuclear.

811 DOI
812 https://doi.org/10.6084/m9.figshare.12844634

813 URL
814 https://figshare.com/s/98b7eb05deaa58d57c4e

Plasmids

expressed cDNA	use	plasmid	Addgene #	contributor
APPL1	cloning	APPL1-pmCherryC1	27683	Christien Merrifield
Nrp1	cloning, expression in LF	pmCherry-mNrp1	21934	Guido Serini
PDGFRα	Cloning, expression in LF	pcDNA5FRT-EF-PDGFRα-EGFPN	66787	Lotte Pedersen
mRuby3	cloning	pKK-mRuby3-TEV	105780	Andrzej Dziembowski
mClover3	cloning	pKK-TEV-mClover3	105795	Andrzej Dziembowski
DYKDDDDK (FLAG)	cloning	pCMV-N-FLAG	--	Takara (commercial)
AktAR2	Akt biosensor	pcDNA3-AktAR2	64932	Jin Zhang
AktPH-GFP	inositol-3 phosphate biosensor	pcDNA3.1-AktPH-GFP	18836	Craig Montell

Antibodies for imaging

antigen	purpose	source	product #	concentration/dilution
APPL1	PLA	Abcam	ab05195	2 μg/ml
EEA1	PLA	Abcam	ab50313	1 μg/ml
GIPC1	PLA	Abcam	ab5951	5 μg/ml
Myosin 6	PLA	Millipore/Sigma	ABT42	2 μg/ml
Nrp1	PLA	R&D Systems	AF566	1 μg/ml
PDGFRα	PLA	R&D Systems	AF-221-NA	4 μg/ml
DYKDDDDK	antibody feeding	Rockland	600-441 or -42-383	2 μg/ml
LAMP1	immunofluorescence	Developmental studies hybridoma bank University of Iowa	cloneIDB4	5 μg/ml

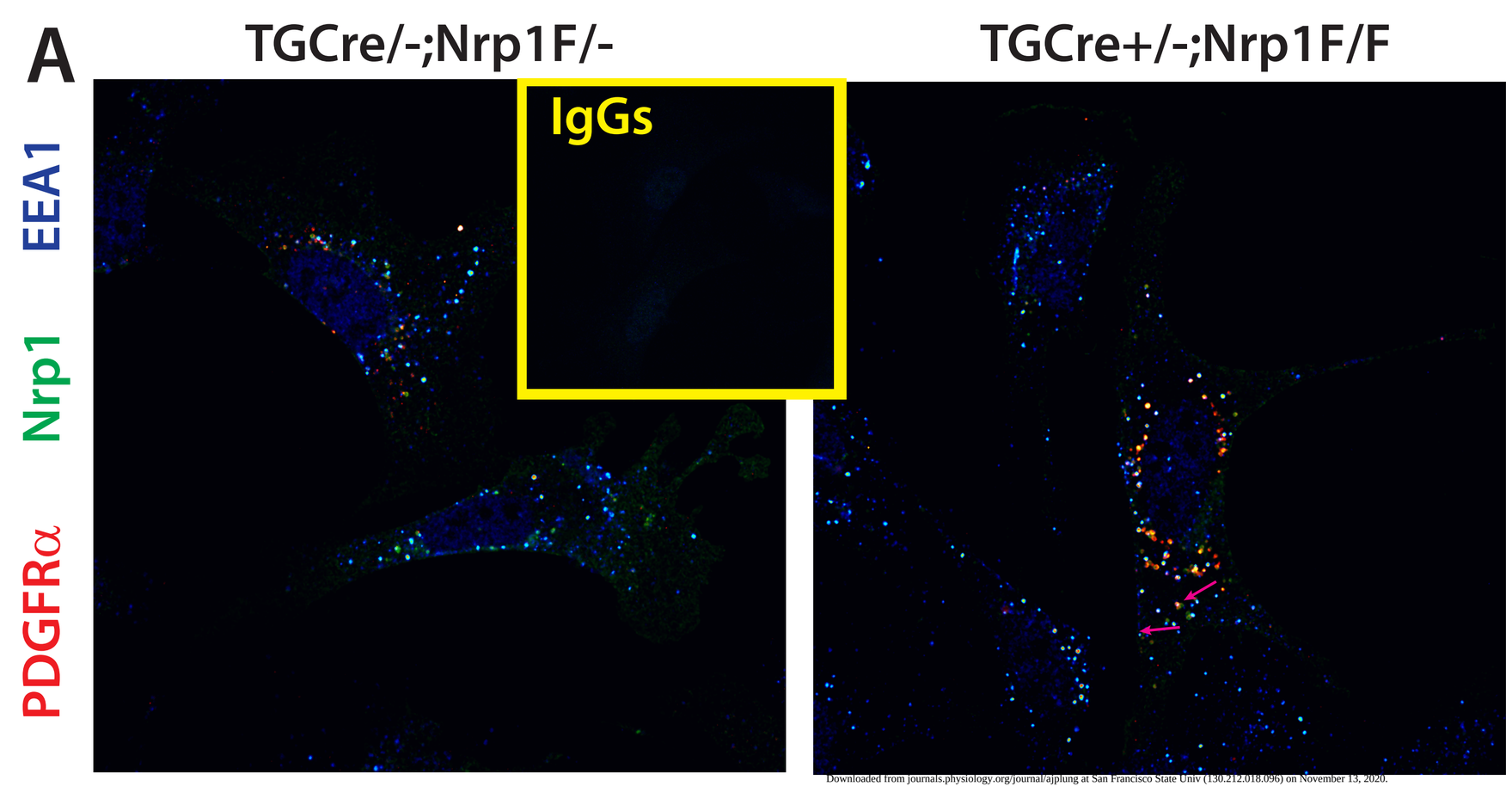

B

Figure 1

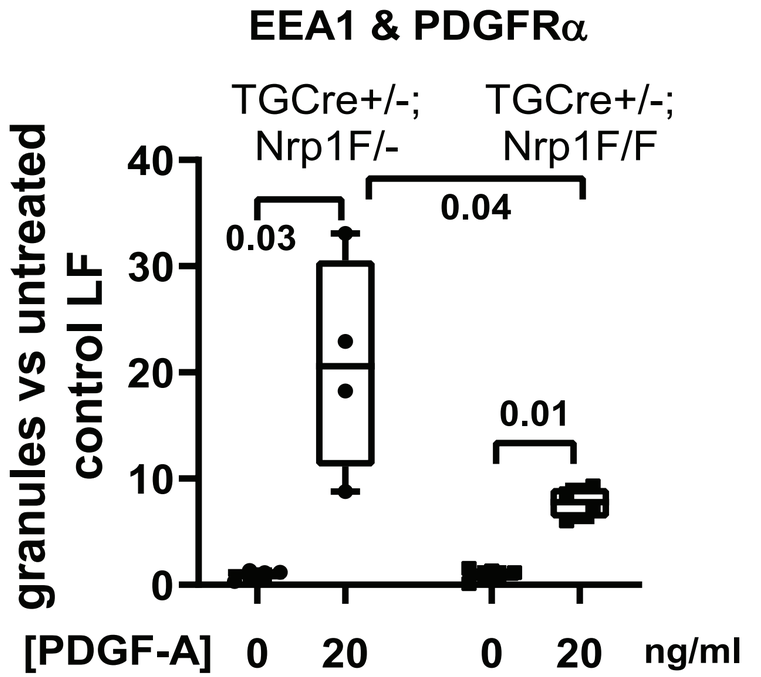

[PDGFA] ng/ml 0 20

A

TGCre+/-;Nrp1F/-

PLA phalloidin nucleus 10 µm

TGCre+/-;Nrp1F/F

B

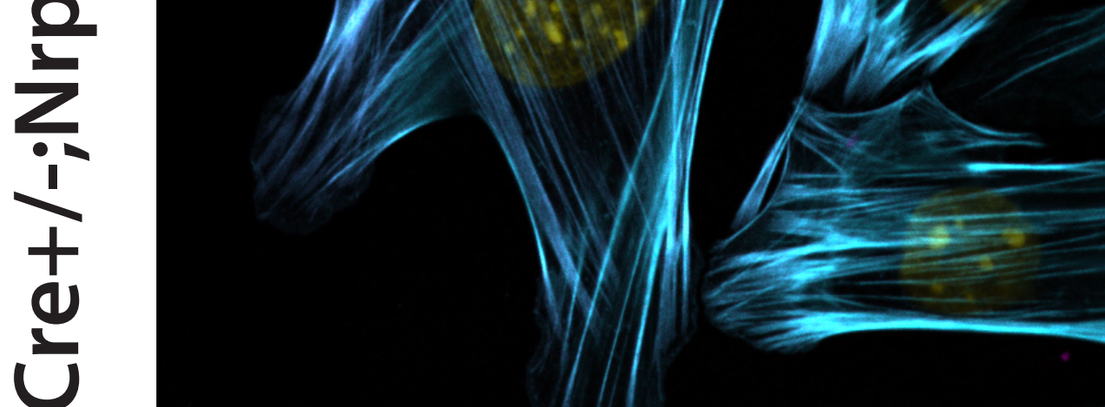

C

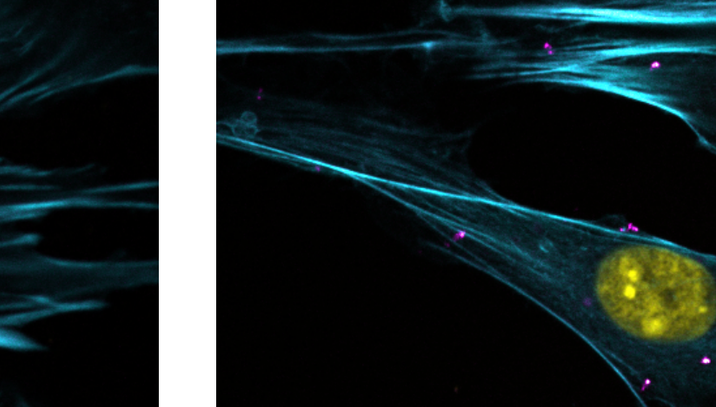

D

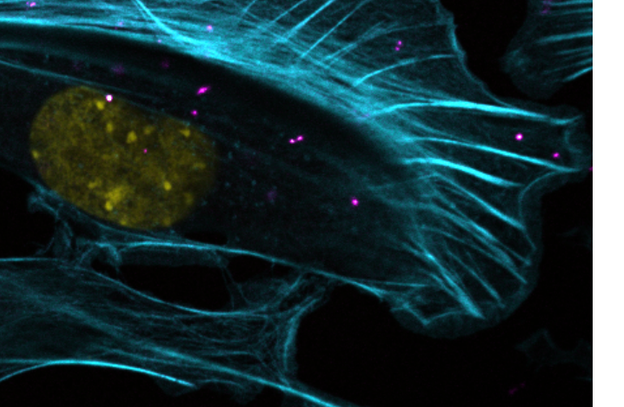

Figure 3

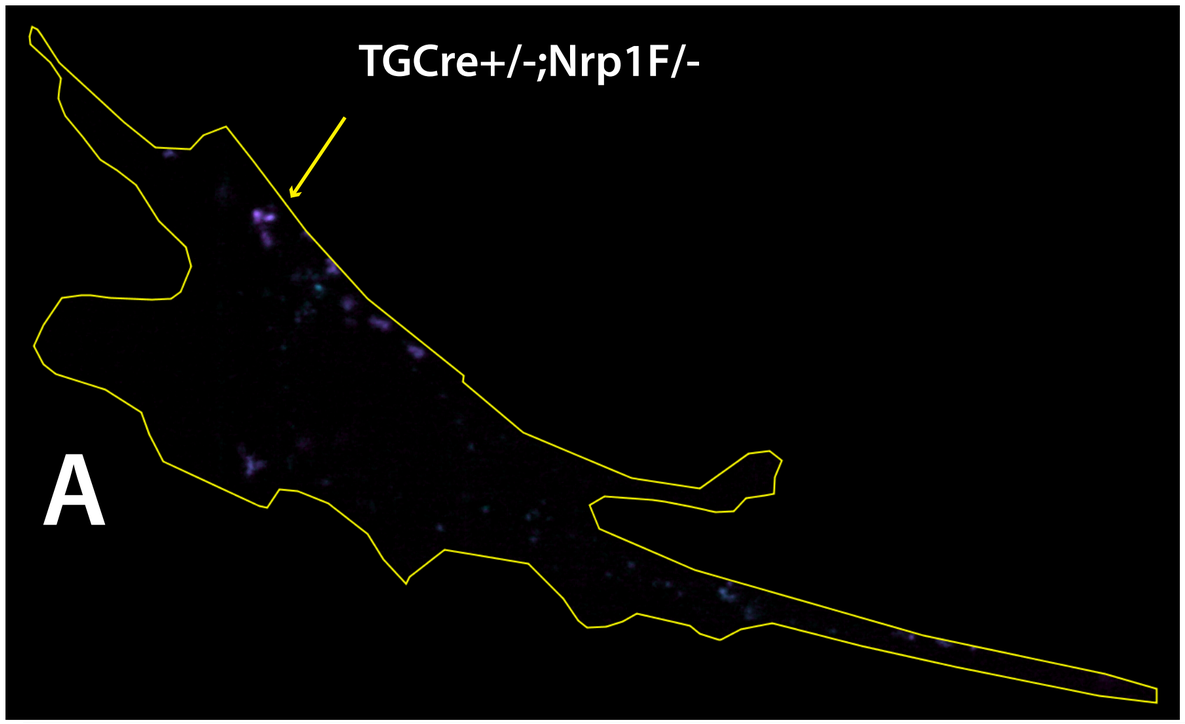
TGCre+/-;Nrp1F/-
A

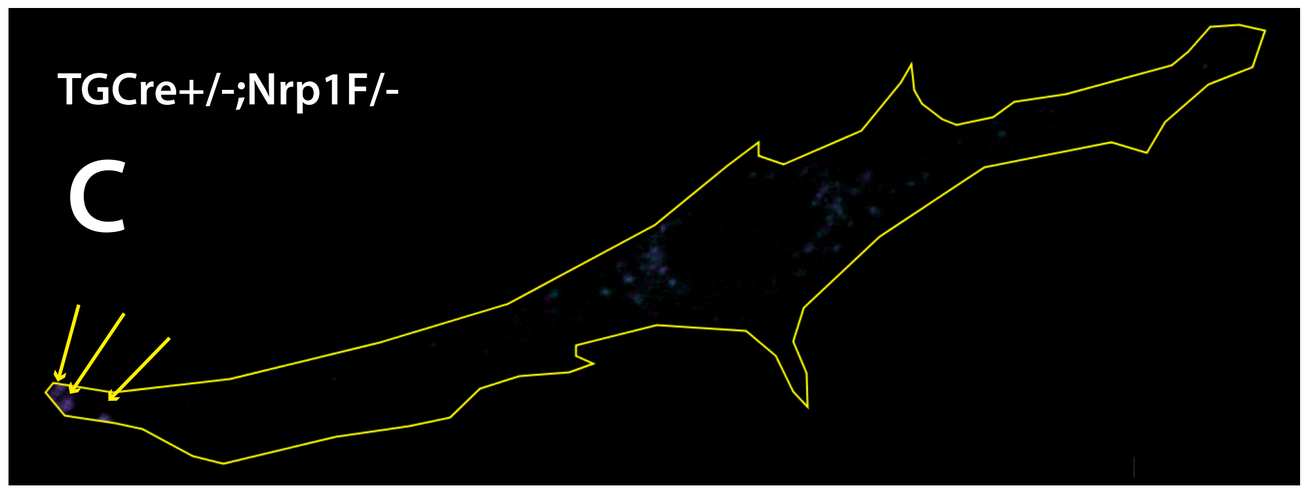
TGCre+/-;Nrp1F/-
C

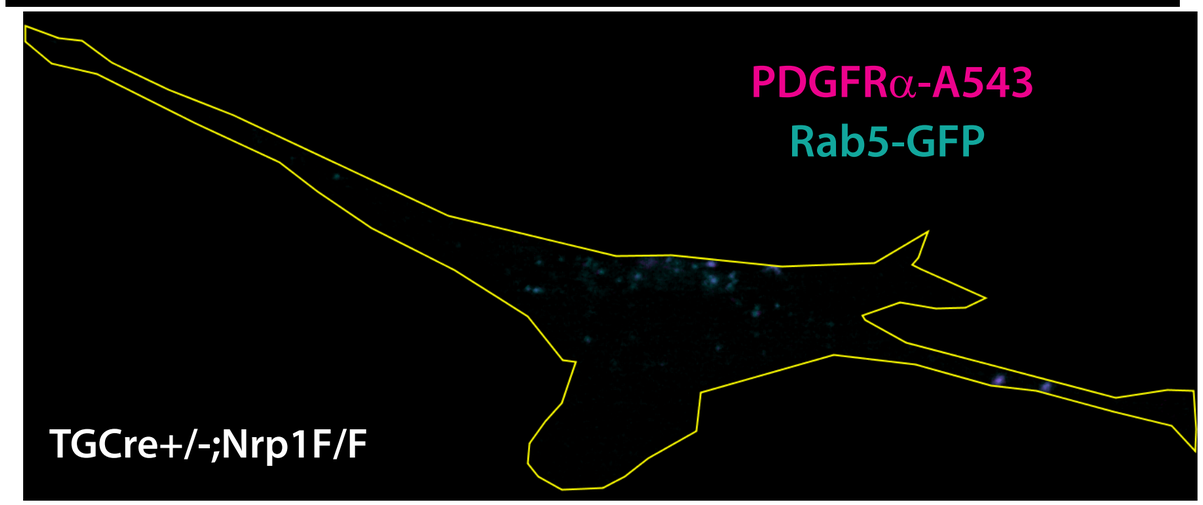
PDGFRα-A543
Rab5-GFP
TGCre+/-;Nrp1F/F

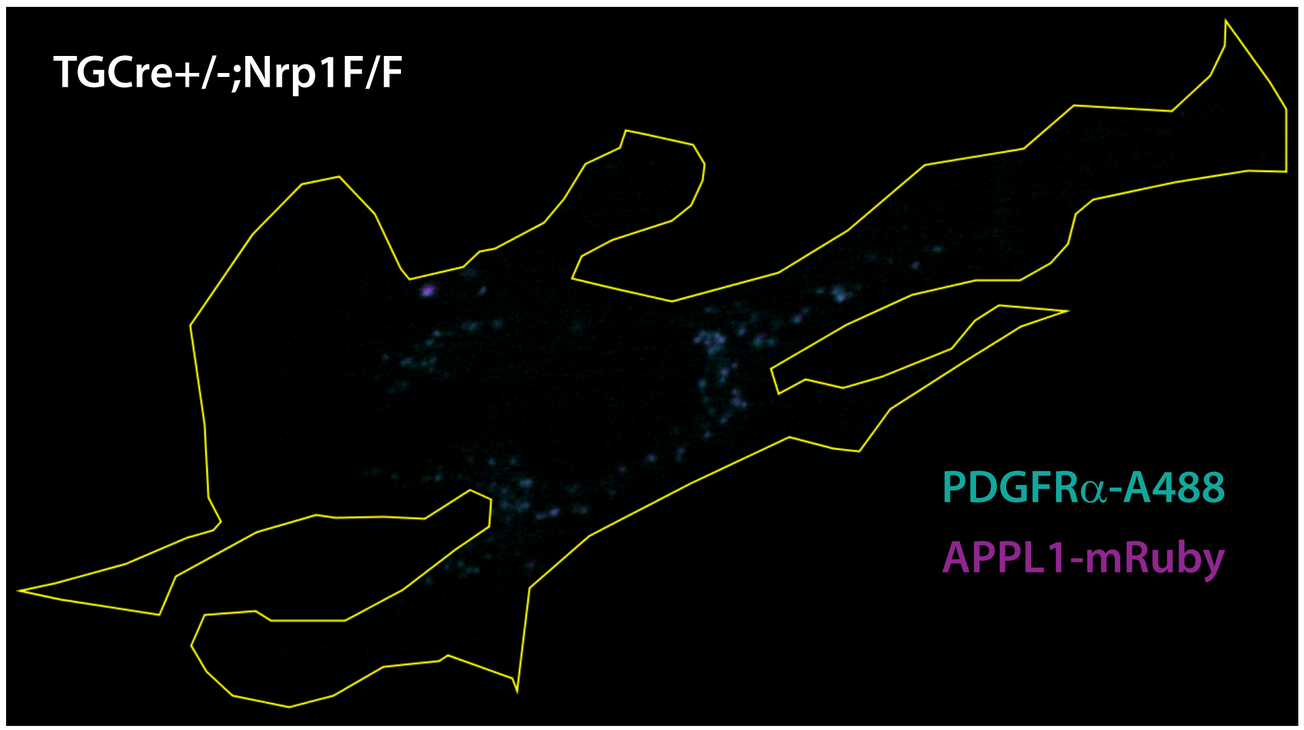
TGCre+/-;Nrp1F/F
PDGFRα-A488
APPL1-mRuby

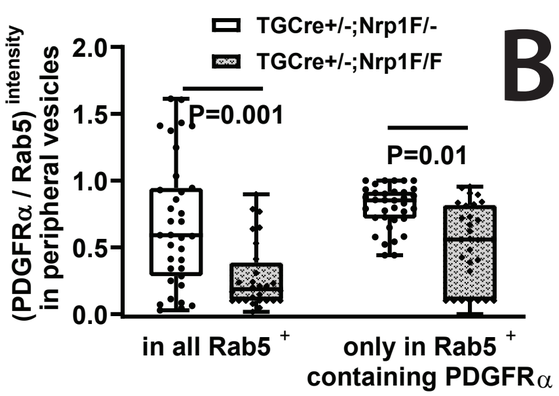
TGCre+/-;Nrp1F/-
TGCre+/-;Nrp1F/F
B
(PDGFRα / Rab5) intensity in peripheral vesicles
2.0
1.5
1.0
0.5
0.0
P=0.001
P=0.01
in all Rab5 +
only in Rab5 + containing PDGFRα

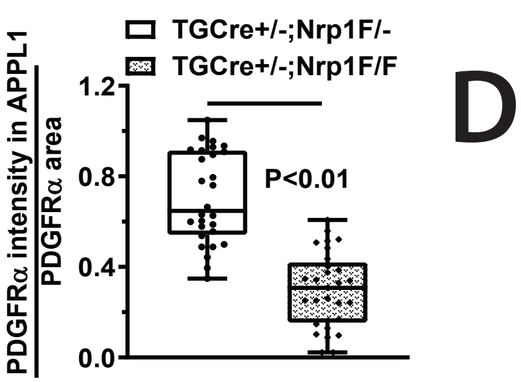
TGCre+/-;Nrp1F/-
TGCre+/-;Nrp1F/F
D
PDGFRα intensity in APPL1
PDGFRα area
1.2
0.8
0.4
0.0
P<0.01

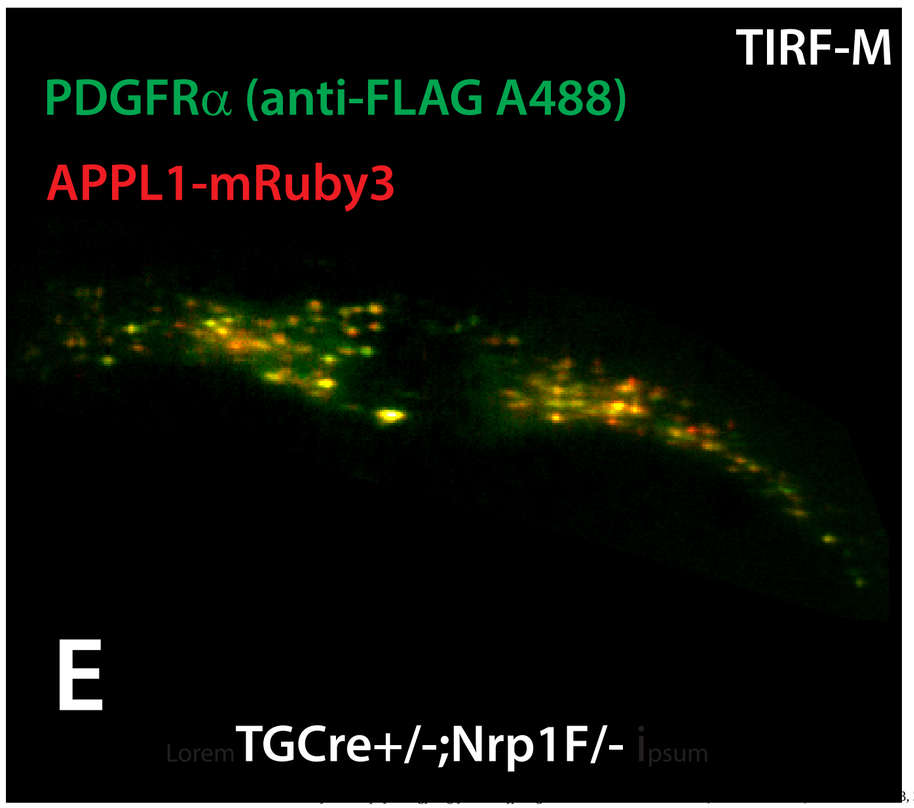
TIRF-M
PDGFRα (anti-FLAG A488)
APPL1-mRuby3
E
TGCre+/-;Nrp1F/-

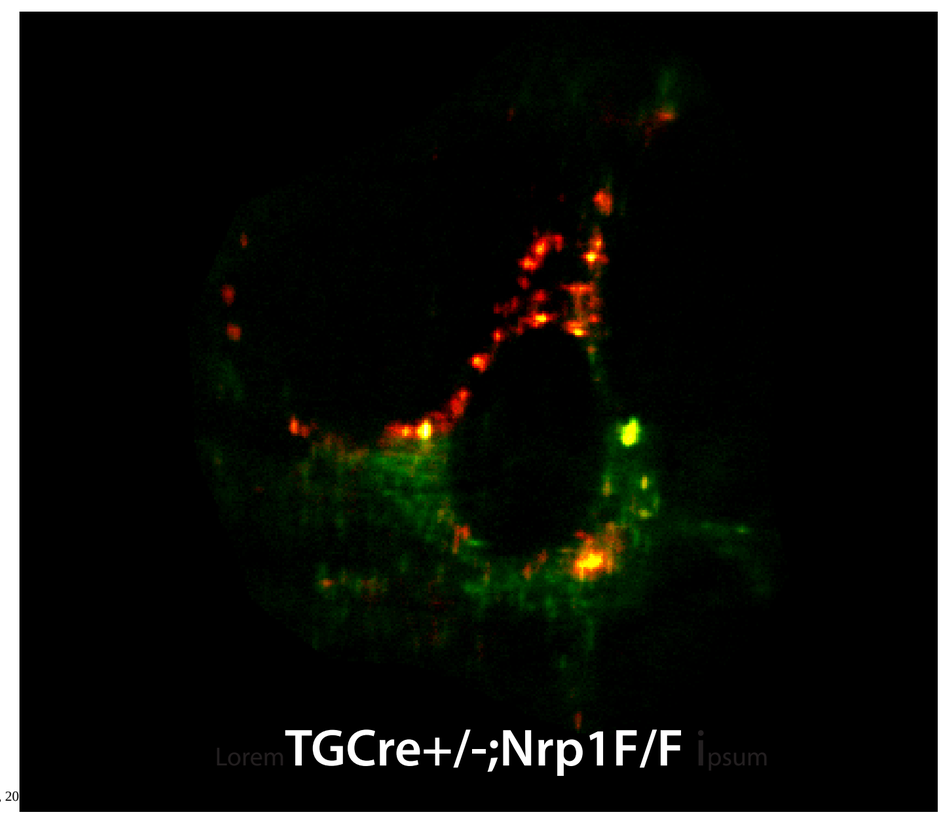
TGCre+/-;Nrp1F/F

Figure 4

[PDGFA] ng/ml 0 20

A

wildtype

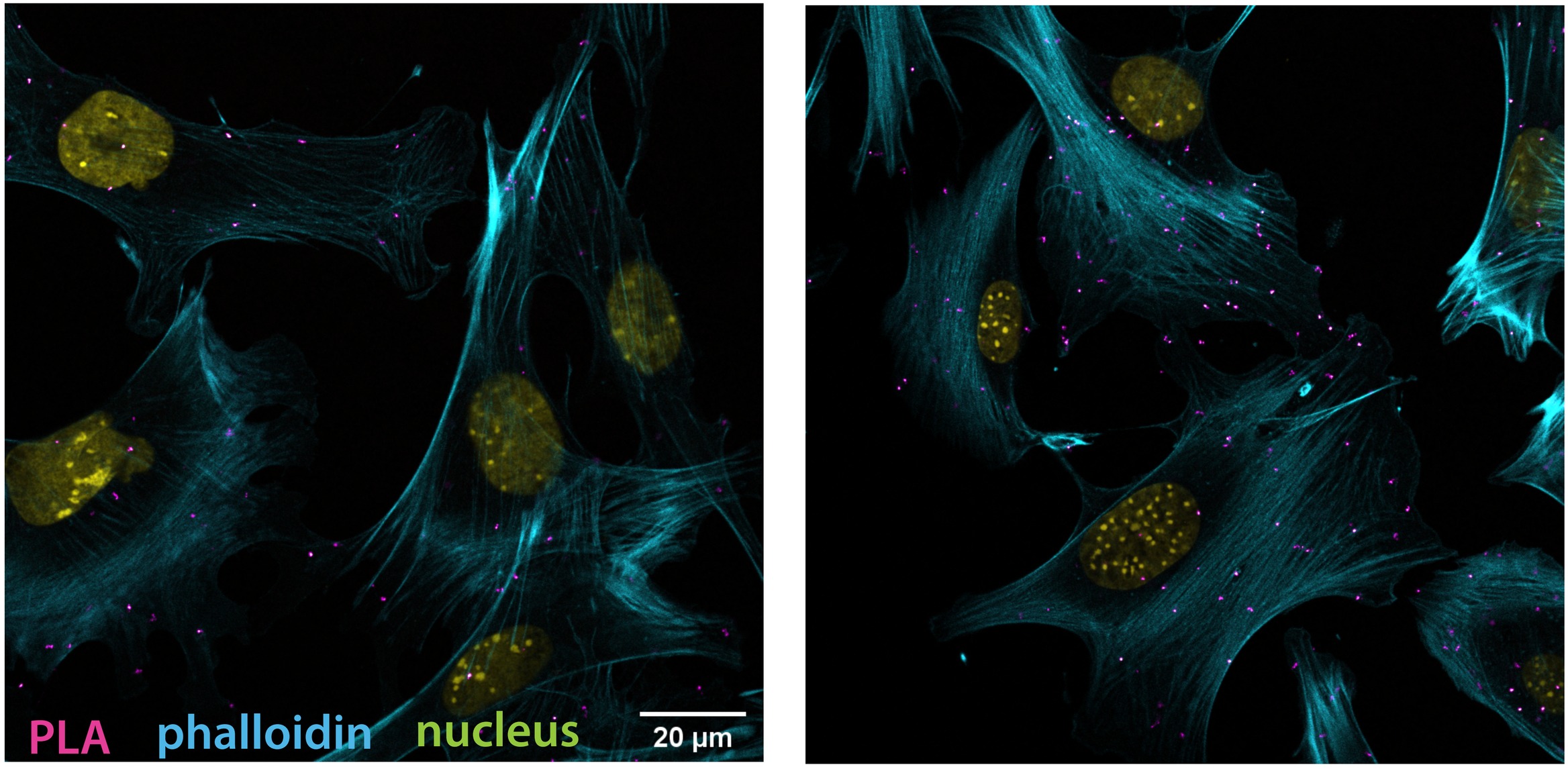

B

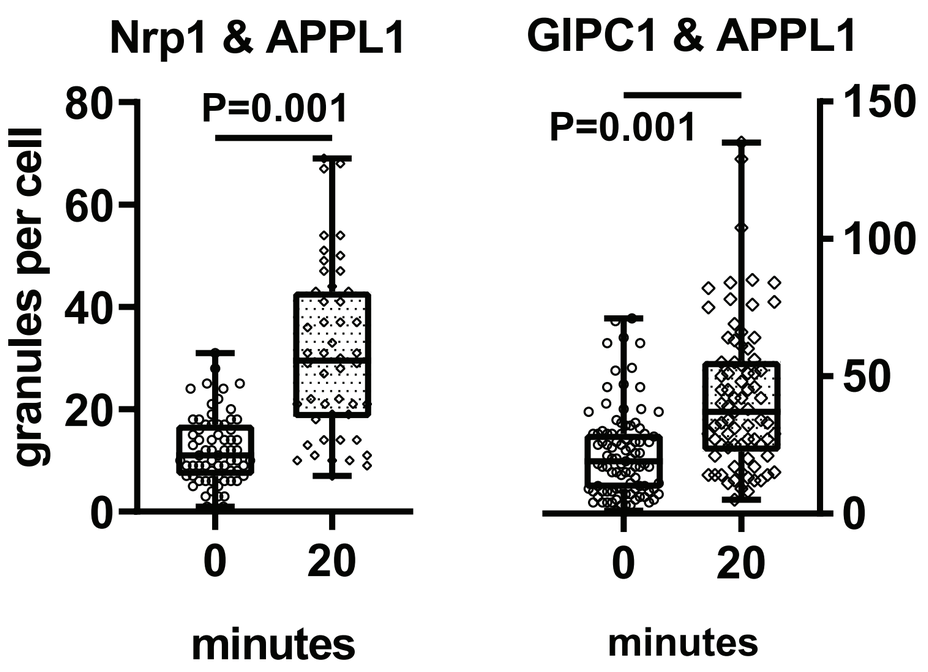

C

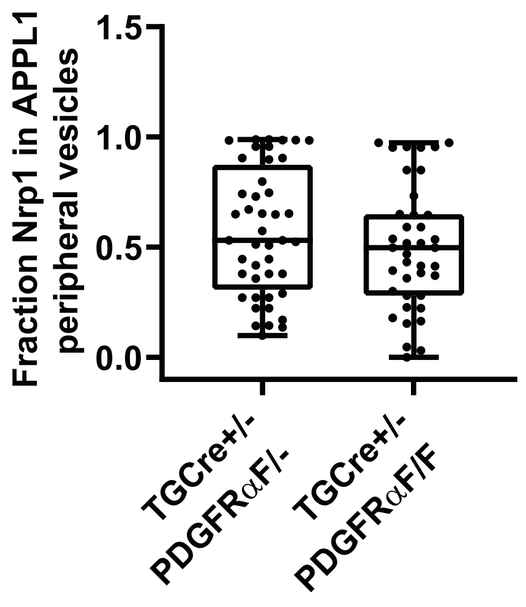

D

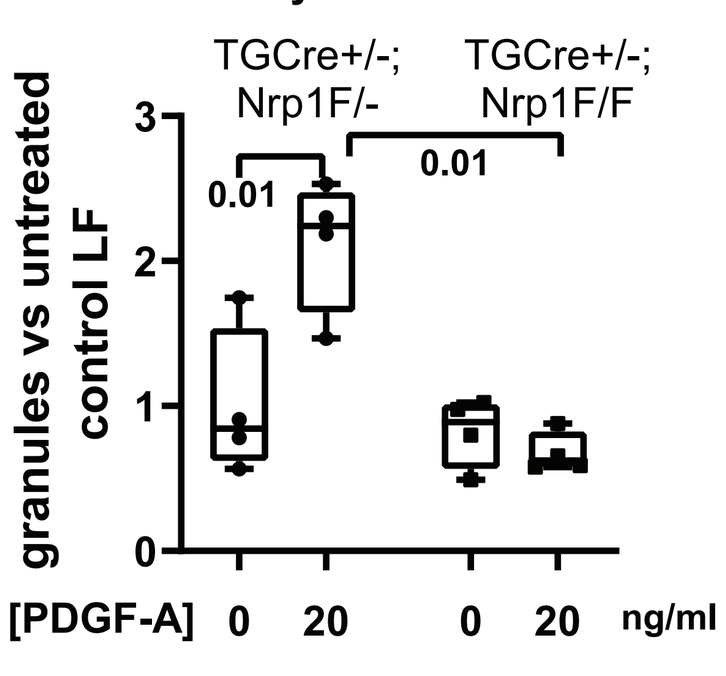

Figure 5

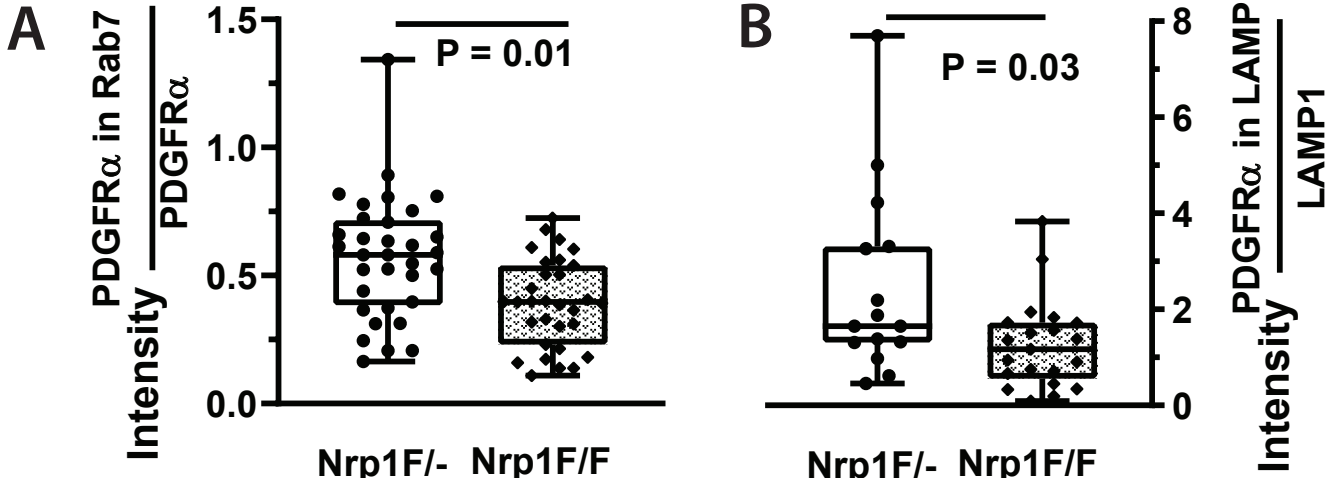

Figure 6

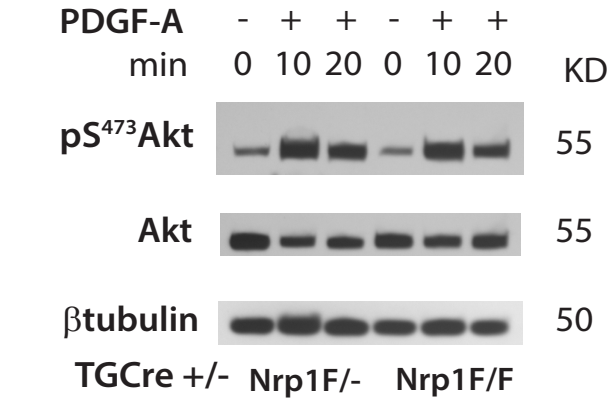

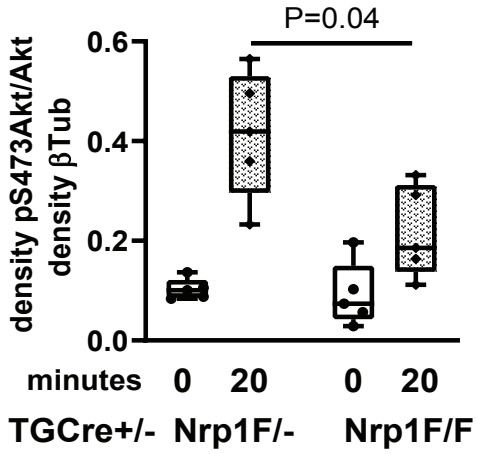

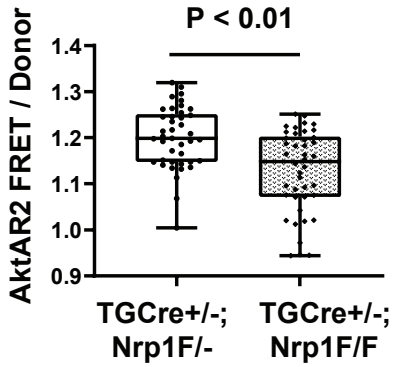

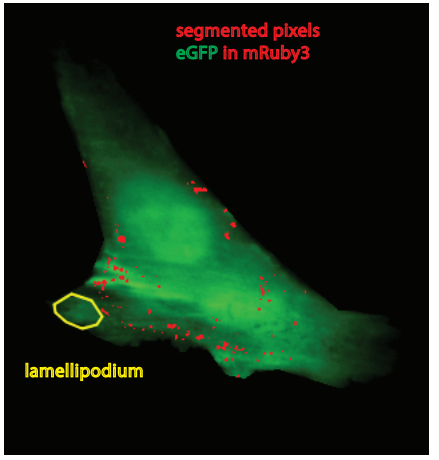

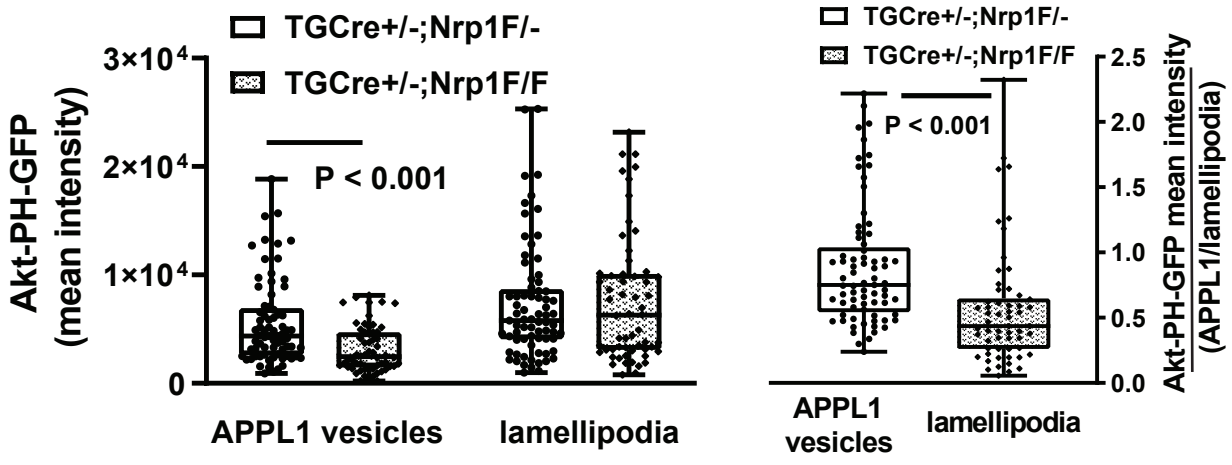

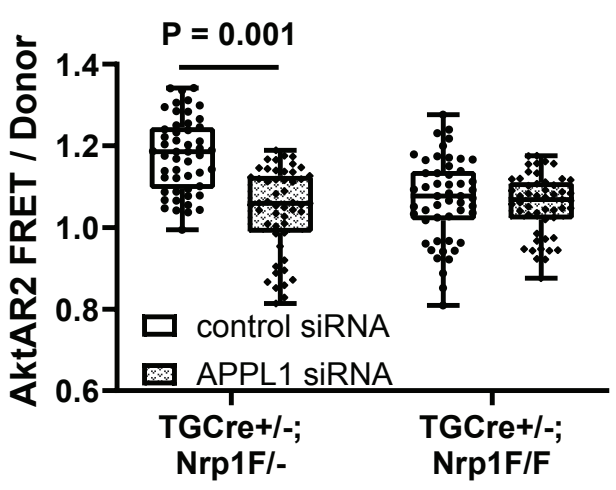

Figure 7